Modelling the Impact of Residual Currents on the Interaction Between Sand Waves and Trenches in Delft3D FM

A case study on Nemo link

C.M.A. (Celine) Bloem

Delft University of Technology

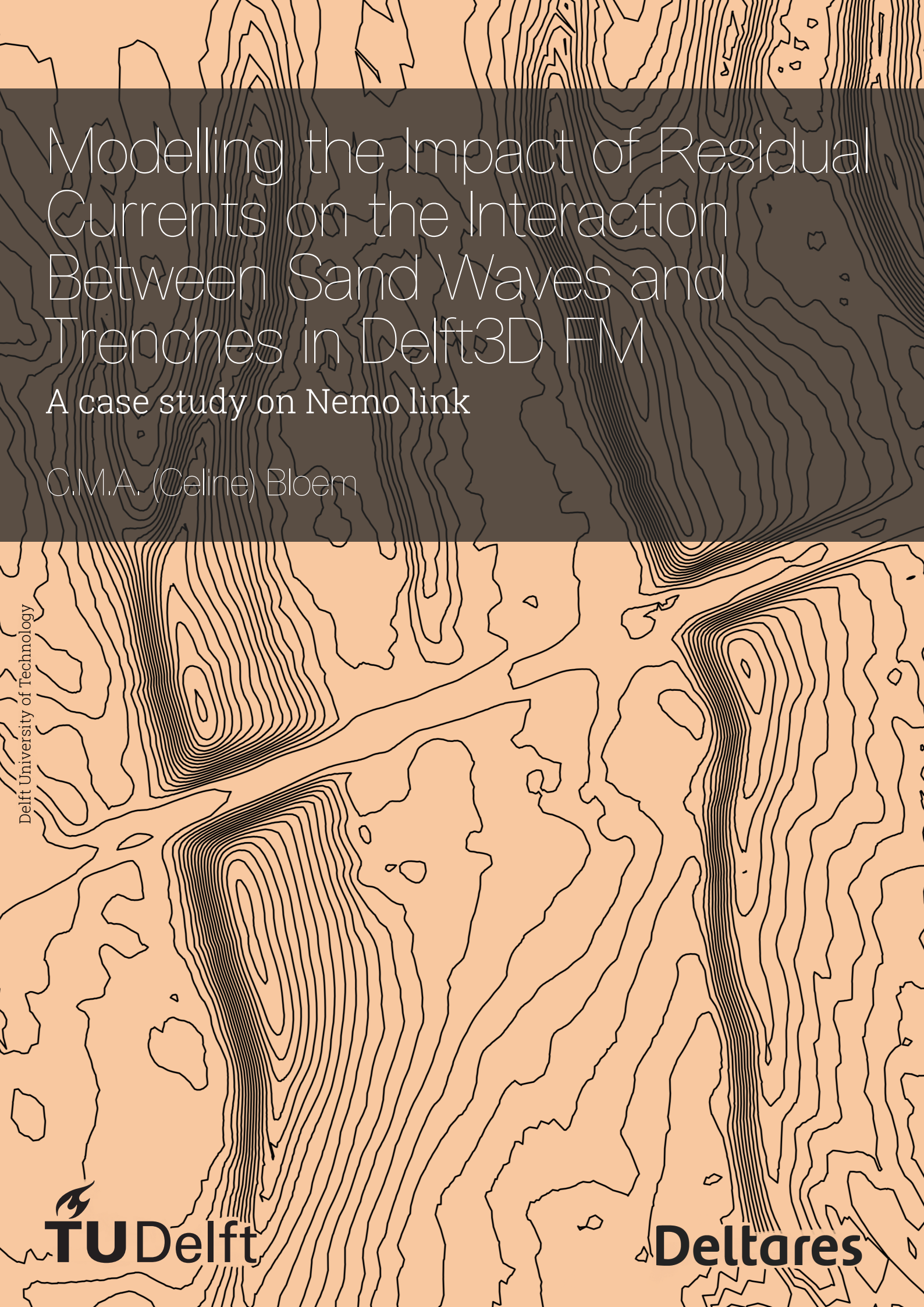

TU Delft

Deltares

Modelling the Impact of Residual Currents on the Interaction Between Sand Waves and Trenches in Delft3D FM

A case study on Nemo link

by

C.M.A. (Celine) Bloem

to obtain the degree of Master of Science
at the Delft University of Technology,
to be defended publicly on Wednesday July 10, 2024 at 14:00.

Student number:	4666607	
Thesis Duration:	February, 2024 - July, 2024	
Faculty:	Civil Engineering and Geosciences	
Thesis committee:	Prof. Dr. ir. A.J.H.M. Reniers,	TU Delft
	Dr. ir. B.C. van Prooijen,	TU Delft
	Dr. ir. A.P. Luijendijk,	TU Delft, Deltares
	ir. P.H.P. Overes,	University of Twente, Deltares

Cover: Isoline plot of a trench through sand wave field
Style: TU Delft Report Style, with modifications by Daan Zwaneveld

TU Delft Deltares

Preface

Before you lies the final effort into obtaining my Masters of Science in Hydraulic Engineering at Delft University of Technology. The thesis marks the end of my time as a student in Delft. I initially started my studies in Applied Mathematics. I soon discovered that the courses I followed were much too abstract for my liking, and for me in order to be motivated about a subject I must be able to see its direct link to practice. I decided to switch to Civil Engineering, and I have never regretted the decision. Not only did I find an abundance of subjects with practical applications, I have also made friends for life. My interest for subjects with real-world applications finally led me to the topic of sand waves, which can pose a nuisance to offshore infrastructure projects. Through this thesis, I hope to have made a meaningful contribution to the field, and I aspire to continue addressing societal challenges in the future.

The thesis would not have been possible without the help of a great many people, to whom I would like to express my gratitude. The thesis builds upon the model developed by Zeta, who was always available for questions which was very valuable to me. My thanks also go out to Deltares, I am grateful for spending my thesis time here and I enjoyed the interactions with colleagues and my fellow graduation interns. Naturally, my gratitude also extends to my graduation committee. Ad, Bram, and Arjen, your enthusiasm is an inspiration and your efforts to have me put the subject in a broader perspective are greatly appreciated. Pauline, during our weekly meetings you have shared your extensive knowledge on the subject of sand waves and I have learned an incredible amount from you. I wish you all the best in the continuation of your PhD and I look forward to hearing more about your work in the future. Finally, I would also like to thank my family and friends. I'm thankful for my friends and all the hours we have spent studying together, you have always managed to put a smile on my face. My thanks also go out to Marly, Ien, Leo, and Frederieke, who have made our house a home. I also want to thank my family, who have always provided me with unconditional love and support. My final thanks go to Mats, who always believes in me.

C.M.A. (Celine) Bloem
Delft, July 2024

Abstract

Sand waves are rhythmic seabed patterns which develop as a result of the interaction between tidal flow and perturbations in the seabed. Due to their size and dynamic behaviour sand waves can pose a threat to offshore infrastructure such as cable trenching. To ensure the safety of these cables, it is crucial to understand the interactions between sand waves and trenches. Residual currents, currents that are not induced by the tide, can exert a significant influence on sand wave dynamics due to the non-linear relationship between flow velocity and sediment transport. Hence, this thesis aims to investigate the effects of residual currents on the morphological interactions between sand waves and trenches. A Delft3D FM model is used to simulate a case study of a trench within a group of sand waves in the Belgium Continental Shelf. The influence of residual currents, mostly induced by wind and atmospheric pressure, is studied during a period of a storm and a period with representative residual currents. It is found that during the tidal cycle at the peak of the storm, the residual currents cause an increase of 66% in sediment infilling into the trench compared to tide-only conditions. Since this is in the same order of magnitude as the background infilling due to tidal dynamics, this is less than expected. The residual currents are however strong enough to reverse the sediment transport patterns of the sand wave and trench system. During the representative residual currents, the contribution of residual currents is found to be insignificant, especially compared to the observed influence of the spring-neap tide. This study concludes that the overall effects of the residual currents, induced by wind and atmospheric pressure, can alter sediment transport patterns but the magnitudes are insignificant in the case study under investigation. It is recommended, for further research and for effective design and maintenance of offshore infrastructure procedures, to keep in mind that morphodynamics of sand wave and trench systems are highly subject to the variations in tidal dynamics induced by the spring-neap tide.

Contents

Nomenclature

General abbreviations

Abbreviation	Definition
2DV	Two-Dimensional Vertical
AOI	Area Of Interest
DCSM	the 3D Dutch Continental Shelf Model in Delft3D FM
Delft3D FM	Delft3D Flexible Mesh
MAE	Mean Average Error
Morfac	Morphological Acceleration Factor
MSL	Mean Sea Level
OREAC	the Ocean Renewable Energy Action Coalition
RMSE	Root Mean Square Error

Abbreviations DCSM simulations

Abbreviation	Definition
AFM	simulation including All Forcing Mechanisms
NTS	simulation excluding Temperature and Salinity
NWA	simulation excluding Wind and Atmospheric pressure
OT	simulation only including Tidal forcing

1 Introduction

The European Union strives for climate-neutrality in 2050. In order to achieve net-zero greenhouse gas emissions, the transition towards renewable energy sources is now in full swing. Offshore wind production is indispensable in this transition and is expected to become the main source of sustainable energy in Europe (Rijksoverheid, 2023). This projected increase in offshore wind energy is not confined to Europe only. The Ocean Renewable Energy Action Coalition (OREAC) envisions a fifty-fold increase of today's global offshore wind capacity by 2050 (Council, 2020). In order to achieve these ambitious goals, the offshore wind industry is expanding rapidly. However, the upscaling of offshore wind is accompanied by many challenges. Amongst others, these challenges involve the morphological interaction between offshore interventions and dynamic bed forms. These interactions can pose a threat to the stability of the offshore structures and the coverage of cables. Failure related to these are among the highest risks involved in offshore wind systems, and can result in significant loss of revenue (Deltares, 2023b). The largest contributor to the uncertainties in the interactions between interventions and dynamic bed forms are sand waves.

Sand waves are rhythmic bed patterns that can grow up to several metres in height (up to 20% of the water column), have length scales up to several hundreds of metres, and can be highly dynamic (Morelissen et al., 2003). A field of sand waves is shown in Figure 1.1. Sand waves are observed all over the world where shallow tide-dominated seas with sandy seabeds are present, locations which are also highly suitable for offshore wind generation. This overlap in (future) wind farm locations and sand wave fields in the North Sea is illustrated in Figure 1.2. More comprehensive understanding of the behaviour of sand waves will reduce the uncertainties that are accompanied with the installation and maintenance of offshore wind systems. Ultimately, this will allow for a safer, more efficient, and smoother transition towards sustainable energy production.

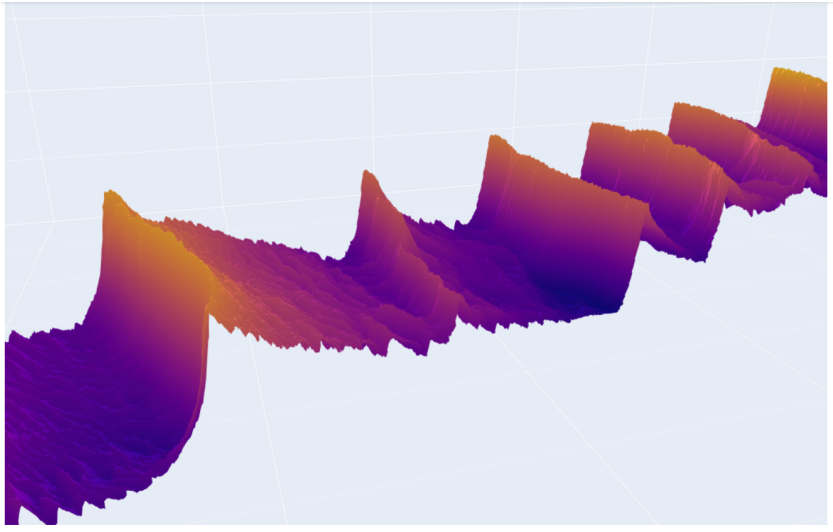

Figure 1.1: A 3D impression of sand waves in the North Sea (vertical scale is exaggerated for illustration) (Tam (2023).

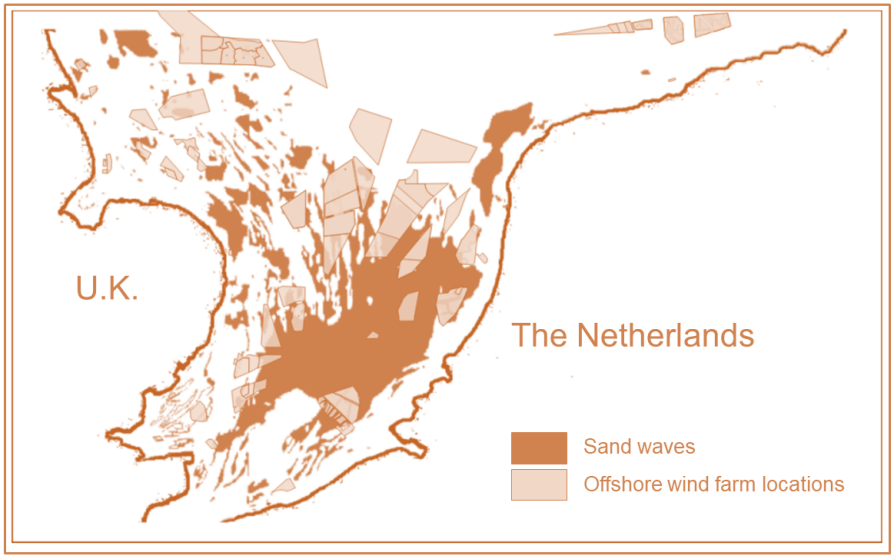

Figure 1.2: A composite image of Offshore Wind Farms Areas and Sand Wave Coverage in the southern North Sea. Adopted from Tam (2023).

1.1. Problem definition

Sand waves develop due to the interaction between seabed perturbations and tidal flow. Hence, many studies that investigate sand wave dynamics tend to focus on the tide as forcing mechanism. There are however publications that indicate the importance of including (time-varying) residual currents in sand wave models in addition to the tidal flow velocities (Campmans, 2018; Overes et al., 2024). In this thesis the term “residual currents” refers to currents that are caused by other forcing mechanisms than the tide. These forcing mechanisms can be wind, (wind-) waves, atmospheric pressure gradients, and density differences. Residual currents induced by these forcing mechanisms can reach up to the seabed. Due to the non-linear relationship between near-bed velocities and sediment transport the residual currents are expected to induce significant morphological changes during peak tidal velocities. This concept is visualised in Figure 1.3.

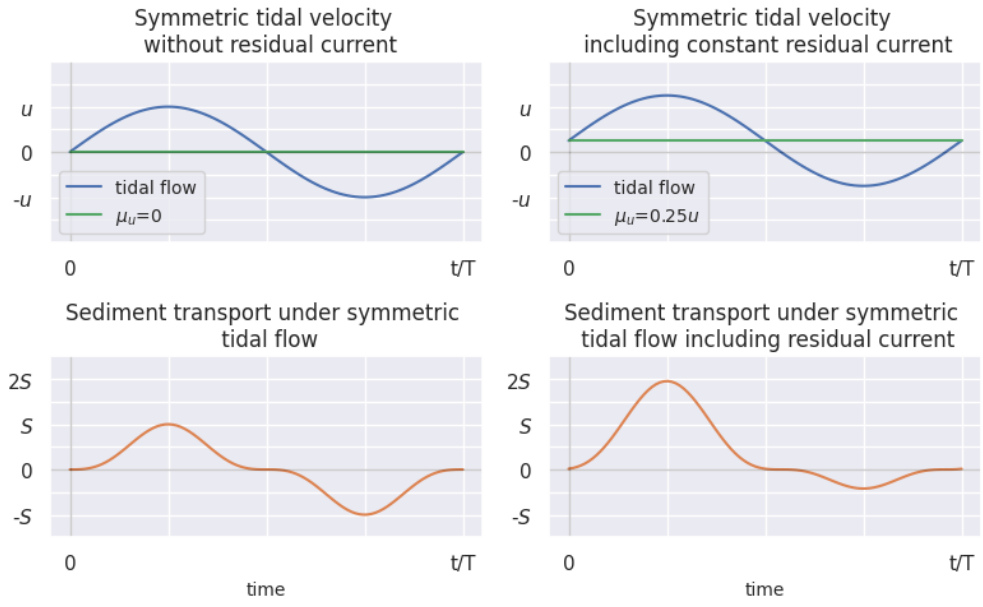

Figure 1.3: Conceptualization of the non-linear relationship between currents and sediment transport. Sediment transport is proportional to higher order velocities ($S \sim u|u|^{n-1}, n = 3, 4$), hence a small increase in residual current can result in a relatively large increase in sediment transport.

Increasing our understanding of the effects of residual currents on the interactions between sand waves and trenches can be very valuable on both the short and the long term. In the short term it is useful to know how big the impact of event-driven residual currents can be on dredging works during the construction phase of offshore wind projects. In the long term, this understanding can be used to predict the envelope of the sand wave behaviour relative to the lifespan of wind farms.

1.2. Research questions

The main research question of the thesis is as follows.

"What role do residual currents play in the morphological interaction between sand waves and trenches?"

In order to find the answers to the main research question a case study is performed. The case study concerns a group of sand waves located in the Belgium Continental Shelf. The sand waves were dredged to allow for the installation of a submarine electricity cable. The project is referred to as Nemo link. Bed level measurements of the Area Of Interest (AOI) are available just after the dredging of the trench in April 2018, and three years after dredging in July 2021. The case study location and sand waves are identical to those studied in the thesis of Tam (2023). The three sub research questions, which are listed below, aim to find an answer to the main research question through the case study.

1. *"What are the characteristics of residual currents in the Area Of Interest over the period of 2018-2021, and which forcing mechanisms induce these currents?"*
2. *"How do event-driven residual currents influence the interactions between sand waves and trenches?"*
3. *"How do residual currents influence the interactions between sand waves and trenches during representative hydrodynamic conditions?"*

1.3. Approach

The main research question is divided into three subquestions, hence the thesis is structured into three parts. An overview of the methods applied in each part is given below.

Part 1. Case study: Residual currents in the Area Of Interest
First, an analysis of the residual currents in the Area Of Interest over the period of 2018 to 2021 is performed. The currents are retrieved from the 3D Dutch Continental Shelf Model (DCSM). The DCSM is a process-based model in Delft3D Flexible Mesh (Delft3D FM), which uses meteorological forcing to hindcast water levels, currents, sea-temperature and salinity levels over the entire Dutch Continental Shelf (including the location of the Area Of Interest). The model is run for four different settings. One includes all forcing mechanisms, one excludes all forcing mechanisms except for the tidal forcing, one excludes salinity and temperature calculations, and one excludes wind and atmospheric pressure forcing. The currents are retrieved from the DCSM at a location close to the Area Of Interest. The residual currents are found by subtracting the currents from the simulation which only includes the tidal forcing from the currents of the other simulations. The residual currents of the simulation which includes all forcing mechanisms are then characterised in terms of magnitude, direction, and probability of occurrence. Additionally, the highest 5% and the remaining 95% of the residual currents are studied, to be able to make a distinction between residual currents that occur sporadically (event-driven), and residual currents that are characteristic to more representative hydrodynamic conditions. Finally, the residual currents of the other simulations are compared to the simulation which includes all forcing mechanisms and a conclusion can be drawn as to which forcing mechanisms are responsible for inducing the residual currents in this area.

Part 2. Numerical modelling: Short-term
In this part of the thesis the effects of event-driven residual currents on the morphological interaction between sand waves and trenches are studied. A period of time is selected in which the highest residual currents are observed in the Area Of Interest over a period of three years. This period of time coincides with a heavy storm (storm Ciara) that passed by the Area Of Interest. A process-based numerical model in Delft3D FM is used to simulate the effects of these residual currents on the Area of Interest.

The model was developed in the thesis of Tam (2023) and is referred to as “NEMO”. Two different simulations are done, the first uses the currents and water levels from the DCSM simulation which only included tidal forcing as boundary conditions and is referred to as the benchmark simulation. The other simulation includes the currents and water levels from the simulation in DCSM which includes all forcing mechanisms. The results are compared by looking at hydrodynamics, and consequent changes in morphodynamics.

Part 3. Numerical modelling: Intermediate-term
Through the use of the same numerical model, the effects of a different set of residual currents is now examined. The timescale of the simulations is increased to a fourteen day period to be able to include an entire spring-neap tidal cycle. The characteristics of the residual currents during the selected period resemble the characteristics of the 95% remaining residual currents during the period of 2018-2021 in the Area Of Interest. Again a benchmark simulation, which only includes tidal forcing, is compared to a simulation which includes all forcing mechanisms.

1.4. Scope

The numerical model used in thesis is limited to two sediment transport mechanisms; bed load transport and slope-induced transport. For simplicity suspended load transport is not considered, as it is not expected to be the dominant mode of transport. It is however recognised that suspended load transport could introduce additional morphological changes to the system as it is known to dampen sand waves and could potentially induce more sediment infilling into the trench.

Aside from this, waves are also excluded in the model simulations. The trench in the case study under investigation is located at 34 metres below Mean Sea Level (MSL). As the orbital velocities of waves are expected to decrease over the depth, it is assumed that the influence of waves is limited. Aside from this, the wave-module is not yet finished in 3D in Delft3D FM, hence it is not possible to include the effects in the NEMO model. It is however acknowledged that waves can influence sand waves systems, Appendix A relates the influence of waves on morphodynamics to the influence of the residual currents in a quantitative manner.

1.5. Structure of the report

After this introduction, the thesis continues with an overview of the relevant literature on the topic of sand waves, trenches, and numerical modelling in Chapter 2. Next, the case study is elaborated upon in Chapter 3, in which the results of the analysis of the residual currents in the Area Of Interest are presented. Chapter 4 dives into the numerical modelling performed in this thesis. First the model settings and different modelling scenarios are discussed, which is followed by the results of the short and intermediate term modelling respectively. Subsequently, Chapter 5 refers to a discussion of the results, and finally the thesis ends with the conclusion and recommendations in Chapter 6.

2

Literature Review

This chapter provides an introduction to the topic of sand waves. First, sand waves and their characteristics and dynamics are discussed. Next, attention is paid to the current knowledge regarding the interactions between sand waves and offshore interventions. Finally, the relevance of using numerical models to simulate sand wave behaviour and ways to do so efficiently are elaborated.

2.1. Sand waves and its dynamics

2.1.1. Sand wave characteristics

Sand waves are rhythmic bed patterns which are observed all over the world in shallow seas. In order for sand waves to exist, sand must be the dominant bed material (Bokuniewicz et al., 1977; Hulscher & van den Brink, 2001) and near-bed (tidal) flow velocities must be strong (Amos & King, 1984). Sand waves can be characterised by their wave height, wave length, spatial occurrence, asymmetry, and migration speed. Damen et al. (2018) extensively studied the occurrence of sand waves in the Netherlands Continental Shelf. Here, sand wave heights vary from 1-10 metres, and sand wave lengths of 100-1000 metres are observed. These are considered as typical orders of magnitudes (Morelissen et al., 2003). There are however locations, such as the Taiwan Shoal, where sand waves with heights up to 25 metres and length scales up to two kilometers have been observed (Bao et al., 2023). Sand wave asymmetry can be described as the ratio of the horizontal length between the crest and the trough of the sand wave (on both sides) and the total sand wave length. Knaapen (2005) has found a positive correlation between asymmetry and migration of sand waves when considering bed load transport. Usually sand waves show migration rates up to several metres per year (Morelissen et al., 2003), however in the Banks Strait in Australia sand waves were found which migrated over 100 metres in nine months (Auguste et al., 2021).

2.1.2. Formation and decay of sand waves

Sand waves develop as a result of the interaction between tidal flow and perturbations in the seabed (Tonnon et al., 2006). When the tidal current encounters a morphological feature such as a bedform, the flow is contracted, and hence accelerates. After the crest of the bedform the flow decelerates again. This results in a near-bed time-averaged flow towards the crest, as is depicted in Figure 2.1.

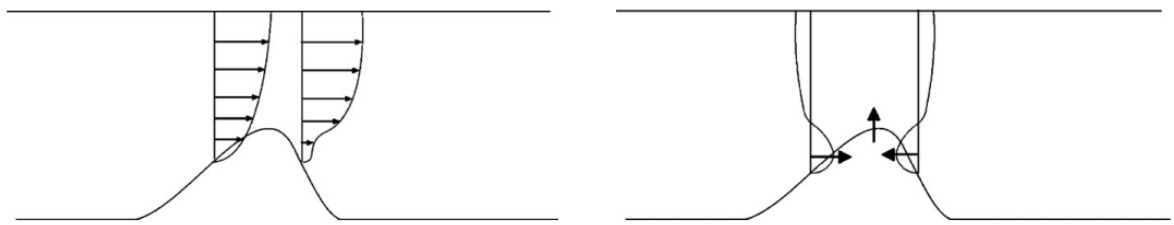

Figure 2.1: Left: velocity profile over a sand wave. Right: Time-averaged (residual) velocity profiles at flanks of the sand wave. Reproduced from Tonnon et al. (2006).

For a symmetrical tide, the time-averaged velocity profile can be schematized as closed circulation cells as depicted in Figure 2.2. The residual tidal currents support the growth of the bedform. The orientation of the sand wave crest is usually perpendicular to the direction of the tide (Hulscher, 1996).

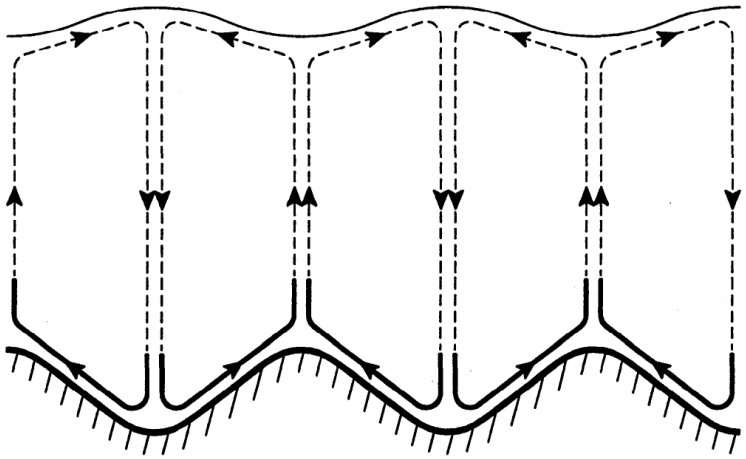

Figure 2.2: Strong near-bed circulation which supports the growth of the bottom perturbation. Reproduced from Hulscher (1996).

The dominant mode of sediment transport influences the growth of the sand wave. Whereas bed load transport enhances the formation of the sand wave, suspended load transport will lead to a dampening of the sand wave according to Borsje et al. (2014) and Damen et al. (2018). The dominant mode of transport is dependent on the Rouse number, which can be determined by the ratio between the settling velocity and the upward motion due to turbulence (Borsje et al., 2014). This ratio is in turn influenced by the characteristics of the sediment; the more coarse the sand, the lower the Rouse number, the more bed load transport can be expected. Additionally, the slope of the bedform also plays a role in the growth of the sand wave. Sand is more easily transported down-slope by gravity, and hence the transport rates are higher in the down-slope direction resulting in a dampening of the sand wave by slope-induced transport. Again, this mechanism is influenced by the characteristics of the sediment. Other environmental parameters that have been reported to influence sand wave characteristics are water depth, waves, tidal asymmetry and residual currents.

2.1.3. Migration of sand waves

Sand waves can migrate due to asymmetries in the tide or due to non-tidal residual currents. The inclusion of higher harmonics in the tidal signal can cause flood or ebb dominance. This will result in a distortion of the circulation cells in Figure 2.2, causing a net migration of the sand wave (Besio et al., 2003). The migration direction of the sand waves is in agreement with the direction of the dominant tidal current. Residual currents can also induce migration of sand waves, and concern all types of currents which are not forced by the tide. Forcing mechanisms that can induce these currents are (wind) waves, wind, storm surge, atmospheric pressure gradients, and density-differences (such as salinity and temperature). Again, the direction of migration of the sand wave is in the direction of the residual current. As bed load transport can be related to higher order velocity moments (Bosboom & Stive, 2023), the larger the residual currents the faster the sand waves migrate. The 2DV model of Overes et al. (2024) has shown that including a non-tidal time-varying current results in significant effects on the erosion and sedimentation rates and hence the migration rate of a sand wave compared to when these currents were left out or when the currents were assumed constant.

2.1.4. Effects of episodic events

As residual currents can be induced by wind, waves, and storm-surge, episodic events such as storms are of high relevance to the formation and migration of sand waves. Campmans (2018) thoroughly

investigated the effects of wind waves and wind-driven currents on sand wave dynamics. Wind waves tend to decrease the growth rate and enhance the migration which is caused by other processes. Wind-driven currents, like other residual currents mentioned above, play an important role in the migration. These currents, when unidirectional, also tend to decrease the sand wave height and sand wave length (Sterlini et al., 2009). This decrease in sand wave height was also observed in the study of Bao et al. (2020), which investigated the effects of a tropical storm on sand waves in the Taiwan Shoal. It was found that the storm smears out small-scale sand waves, and erodes the crests of giant sand waves. Moreover, the sand waves did tend to recover after the storm.

2.2. Trenches and sand wave recovery

2.2.1. Trenches

As sand waves can be highly dynamic, these bed forms can pose a threat to all human interventions taking place on the seabed. Threats to these activities involve the infilling of dredged trenches before cable installation, the exposure, and the potential damage of the cables. Especially the recovery timescales of the sand waves involved, and the magnitude of the regrowth (the degree to which the areas designated for cable installation remain untouched), and the sediment budgets are of great importance.

2.2.2. Observations of sand wave recovery

In designing dredging strategies for trenches in sand wave fields, it is valuable to know whether or not the sand waves will regenerate. And if they recover, how they will recover and what processes are governing in this regeneration process. Larsen et al. (2020) thoroughly examined sand wave recovery in two dredged trenches at different construction sites of the Race Bank Offshore Windfarm in the UK. The sand waves in the two areas differed in orientation, migration speeds (the sand waves of Area 1 have a higher mobility than those in Area 2), and overall morphology, however the hydrodynamic conditions at the sites were similar. The two different sites are depicted in Figure 2.3.

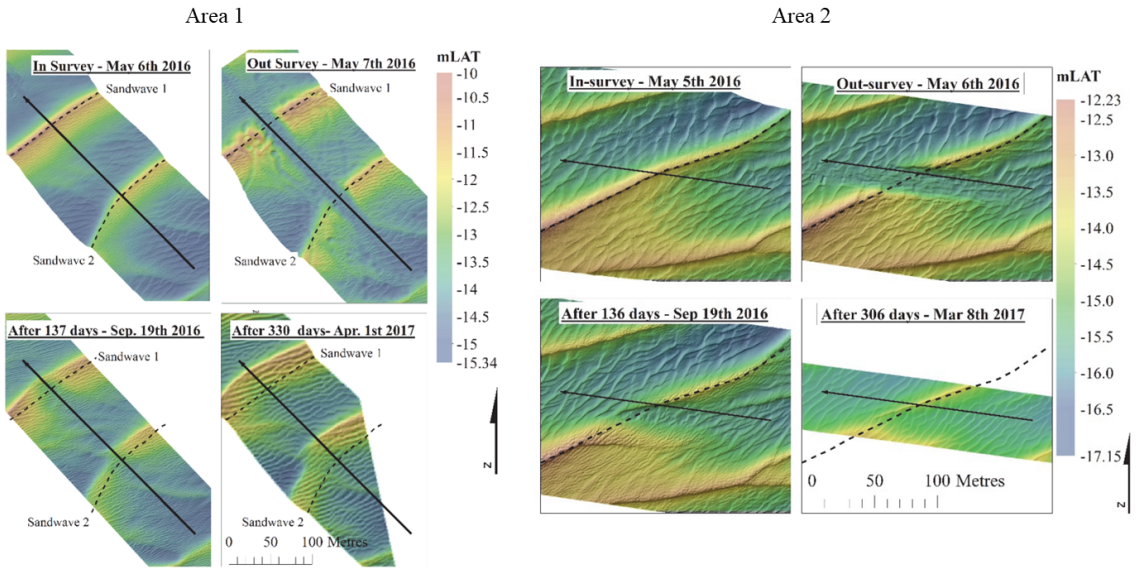

Figure 2.3: Multibeam echo sounding surveys of Area 1 and Area 2. Dashed lines are sandwave crests at time of in-survey. Reproduced from Larsen et al. (2020).

It was found that the regeneration of the sand waves follow an asymptotic exponential form, as is shown in Figure 2.4. Additionally, sand waves in areas with higher bedform mobility are expected to experience shorter recovery timescales.

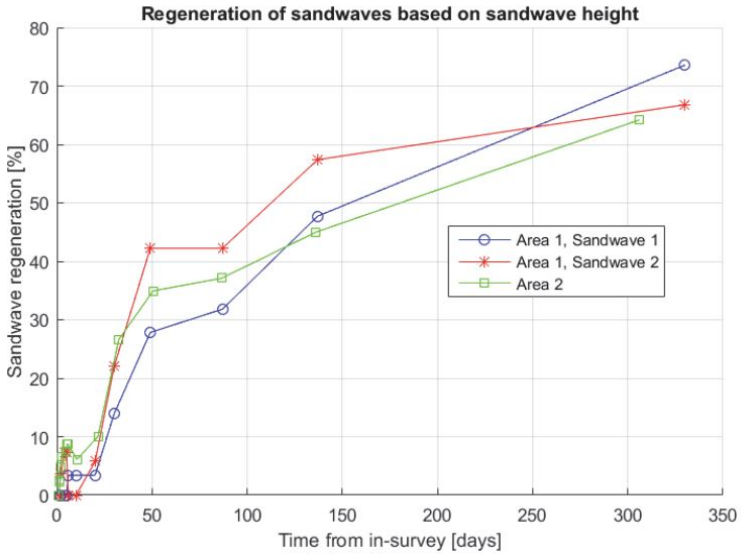

Figure 2.4: Sand wave regeneration in percent based on sand wave heights. Reproduced from Larsen et al. (2020).

In preparation of the planned Offshore Wind Farm project Hornsea 3, Ørsted also investigated these datasets and combined these with bathymetry data of other dredged areas in the Race Bank Offshore Windfarm. From the Sandwave Clearance Clarification Note (Ørsted, 2018) it was concluded that the main factors governing the recovery potential of sand waves after dredging are the configurations of the dredged areas (width and depth relative to sand wave height, and the alignment of the trench to the crest), and the degree of sediment mobility at the dredged location. Additionally, from these measurements, it was observed that the seabed dropped in the areas near the dredging sites. This behaviour is also observed in the recovery of the sand waves that were studied in Tam (2023). Here the influence of sediment infilling into the dredged area was observed up to 100 m to the north and to the south of the trench. This stresses that there is an interaction between dredged and non-dredged area, and that these systems should be considered in a 3D setting. Moreover, in the thesis of Tam (2023) it is also found that sand waves can lose the consistency of their ridge shape. This can be seen in Figure 2.5, where a bifurcation has formed. Such a tail can also be observed when looking at Area 2 of Larsen et al. (2020) in Figure 2.3. It is speculated that the formation of these tails can be attributed to dredging activities.

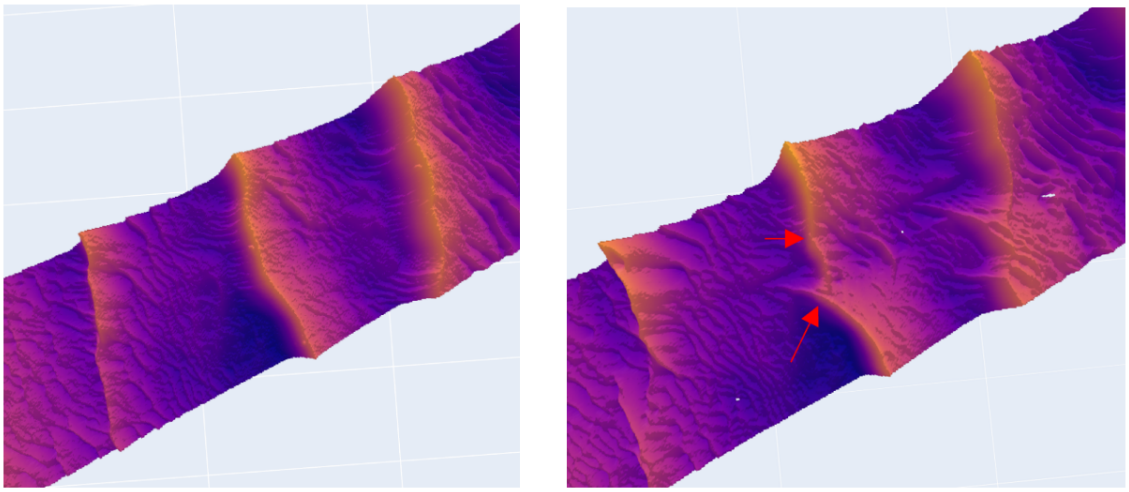

Figure 2.5: Evolution of Sand Wave recovery. Left: Sand Waves prior to dredging (2016). Right: Sand Waves post dredging (2021). Reproduced from Tam (2023).

Krabbendam et al. (2022) studied three former sand extraction sites on the Belgian Continental Shelf, and it was found that sand waves do not always regenerate within a few years of dredging. It is hypothesised that this can be attributed to differences in mean water depths and local sand availability (of erodible sand). Bao et al. (2023) also looked into sand wave recovery in the Taiwan Shoal. In this study, five measurements in eight years time were examined closely of an area in which giant sand waves (5-25 metres in sand wave height) and smaller sand waves (up to 5 m in sand wave height) are present. Two giant sand waves were dredged and it was found that these sand waves partially recover through smaller sand waves. Additionally, it was found that smaller sand waves in the vicinity of the larger dredged sand waves started to migrate in the opposite direction after dredging of the giant sand waves while their asymmetric shapes remained unchanged.

2.2.3. Processes behind sand wave recovery

The thesis of Tam (2023) explores sand wave dynamics after the pre-sweeping in a 3D setting in Delft3D FM. It was found that the transverse slope effect and direct filling by flow are two main contributors when it comes down to the sediment infilling in dredged trenches. Campmans et al. (2021) investigates two types of dredging strategies of sand waves, so-called “topping” and “swiping”, through a non-linear 2DV process based sand wave model. Both strategies entail the partial removal of the crest of the sand wave; during “topping” the sediment is removed from the system, and during “swiping” the material is placed at the trough. In general it was found that the larger the volume of the dredged part, the longer it takes for the sand wave to regenerate. Additionally, the swiping technique proved more effective in terms of recovery timescales than the topping technique for the same volumes of sediment.

2.3. Sand wave modelling

Modelling sand waves creates insights into the contribution of specific processes on the behaviour of a sandy system, this results in increased understanding. Aside from this, models can also be used to predict future behaviour of sand waves, which can be very useful for the planning of offshore infrastructure. There are numerous modelling methods to simulate sand wave dynamics, each with their own (dis-) advantages. A modelling technique that has been proved to generate promising results are process-based numerical models such as Delft3D. These models are based on the underlying physical processes, meaning that these could be more widely applied than for instance data-driven models, for which historic data of the morphological system of interest is required. Delft3D allows for sand wave modelling in two-dimensional vertical (2DV) and three dimensions (3D). Leenders (2018) studied the effects of seabed morphology in an idealized and in a realistic sand wave model setting using Delft3D-4 in 2DV and 3D. During the realistic model study, computational errors were discovered at the boundaries of the sub-domains. These errors can be attributed to grid refinements which are needed to model the transition between the different domains in Delft3D-4. In the meantime, a new version of Delft3D, called “Flexible Mesh” (FM), has become available. Through the use of unstructured grids and parallel computing ability, this version is considered an interesting alternative to Delft3D-4. Overes (2021) reported on the performance of Delft3D FM in simulating sand waves in 3D, and found that the inclusion of a third dimension in sand wave modelling allows for a better representation of variations in flow velocity and direction over sand wave fields. The thesis of Tam (2023) investigated a sand wave and trench system in 3D using Delft3D FM. Here it was observed that the sand waves were not able to maintain their shape, and showed a smoothening of the features. The cause behind this observed behaviour is still unknown, but several numerical and physical reasons are discussed that could be the potential source of the problem.

2.3.1. Efficient modelling

High spatial and temporal scales are required to capture the relevant processes associated with sand wave modelling. Typically, these scales result in large computational efforts (Borsje et al., 2013). Hence, the need for modelling techniques that accelerate morphological changes whilst maintaining accuracy becomes evident. Morphodynamic acceleration techniques are (generally) based on the assumption that hydrodynamic processes occur on much shorter timescales than morphological changes. This allows for the use of the Morphological Acceleration Factor (morfac), a widely applied upscaling technique, which accelerates morphological change with a certain factor. The morfac can be very useful when working with systems in which only the tide is considered, as the tide can be simplified to a

repetitive process. Non-tidal flows unfortunately do not typically show these repetitive features, making the implementation of the morfac less straightforward. Other upscaling techniques include the schematisation of hydrodynamic boundary conditions, also referred to as input reduction. Schematisations of hydrodynamic boundary conditions can be achieved by filtering the conditions (only the conditions are selected for which morphological change occurs), or by making use of the representative weather conditions (selecting the weather conditions that have the highest frequency). Luijendijk et al. (2019) explores a set of morphodynamic upscaling techniques and their results on shorter and longer timescales. Amongst these, a novel modelling technique referred to as “Brute Force Merged” proves an interesting approach to model sandy systems on both a short and long timescale. This technique allows simulations with compressed hydrodynamic boundary conditions to be run in parallel, and merges the bed level changes afterwards.

2.3.2. Delft3D Flexible Mesh

Delft3D Flexible Mesh (Delft3D FM) is a process-based numerical model developed by Deltares and is able to, amongst others, simulate hydrodynamics, sediment transport, and morphology and the interactions between these processes (Deltares, 2023a). Delft3D FM allows for modelling using unstructured grids and is able to compute simulations in parallel, contributing to a decrease in computational times compared to earlier versions. The most important equations and concepts of Delft3D FM are listed here, however for a more detailed overview the reader is referred to the user manual (Deltares, 2024). The computations done in Delft3D FM are based on the computational loop depicted in Figure 2.6. Within one computational step, first the hydrodynamic processes are calculated and next the sediment transport processes are calculated. This is followed by the update of the bed level according to the net fluxes in sediment transport. The process then repeats itself, and the hydrodynamic and sediment transport processes are calculated again by taking the new bed level into account. The D-FLOW FM module within Delft3D FM is used to calculate the hydrodynamics. This is done by solving the continuity equation and the 3D non-linear shallow water equations.

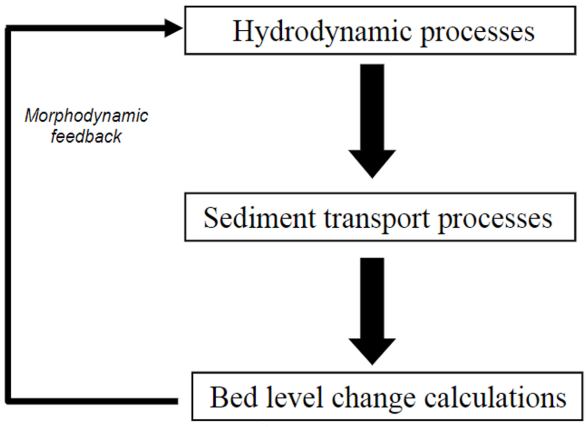

Figure 2.6: General structure of coastal morphodynamic model. Adopted from Ranasinghe et al. (2011).

Sand wave modelling in Delft3D FM

The D-Morphology module within Delft3D FM is used to model sediment transport. The module supports both bed and suspended load transport of non-cohesive sediments. Different formulations can be used to model sediment transport, such as Engelund-Hansen (1967) and the Van Rijn (1984, 1993, and 2007) formulations. After the bed load transport is computed, the Exner equation is used to calculate the bed level change. In this equation the bed load transport can be adjusted by the use of bed slope parameters in streamwise and transverse direction. Choy (2015) thoroughly investigated the influence of these sediment transport formulations and parameters on sand waves. She found that Van Rijn (2007) showed most promise in modelling the growth of offshore sand waves.

3

Case Study

This case study is used to study the interactions between sand waves and trenches more closely in a real-life case and to be able to compare these findings to those computed with the numerical model later in the thesis. The chapter begins with a general description of the context of the dredging activities and the behaviour of the sand waves over the years that bathymetry data was available. Hereafter, the hydrodynamics at the location are studied more closely. This is done through the use of the 3D Dutch Continental Shelf Model (DCSM), of which the settings are discussed first. This is followed by the results of the analysis of the residual currents.

3.1. Description of the Area Of Interest

The case study considers a group of sand waves in the tidally-dominated Belgium Continental Shelf (Vindenes et al., 2018). In April 2018 a trench was dredged through the sand waves to allow for the installation of a submarine power cable. The power cable, referred to as Nemo Link, is roughly 140 km long and transfers electricity from Richborough in the UK to Zeebrugge in Belgium and back (Link, 2013). In preparation of the placement of the cable, several bathymetry surveys with a resolution of 1x1m were conducted by the Nemo Link project (National Grid (UK) and Elia (BE), 2018). Aside from this, the open source dataset EMODnet also has some high resolution (again 1x1m) bathymetry surveys available in the desired period (EMODnet, 2021). An Area Of Interest (AOI) is chosen and five sand waves within this area are selected for further research. The Area Of Interest is roughly 1100 m long in the longitudinal direction and 200 m wide in the transverse direction, and it is aligned along the 255°N axis. Figure 3.1 refers to the exact location of the Area Of Interest, and Figure 3.2 to the enumeration of each of the five sand waves.

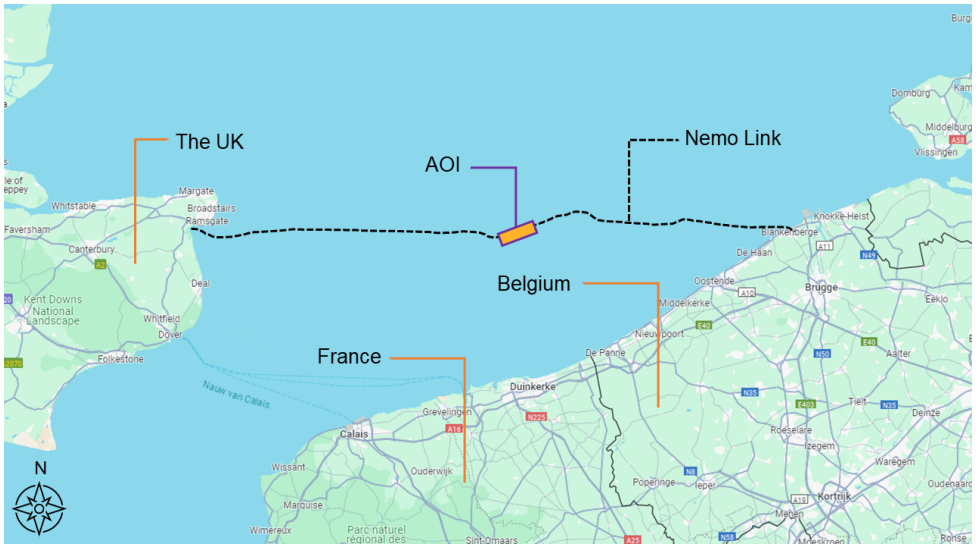

Figure 3.1: Google Maps location of AOI. Adapted from “Google Maps” by Google, n.d. (https://www.google.com/maps/@51.2116015,2.0788078,9.25z?entry=ttu). Copyright by Google.

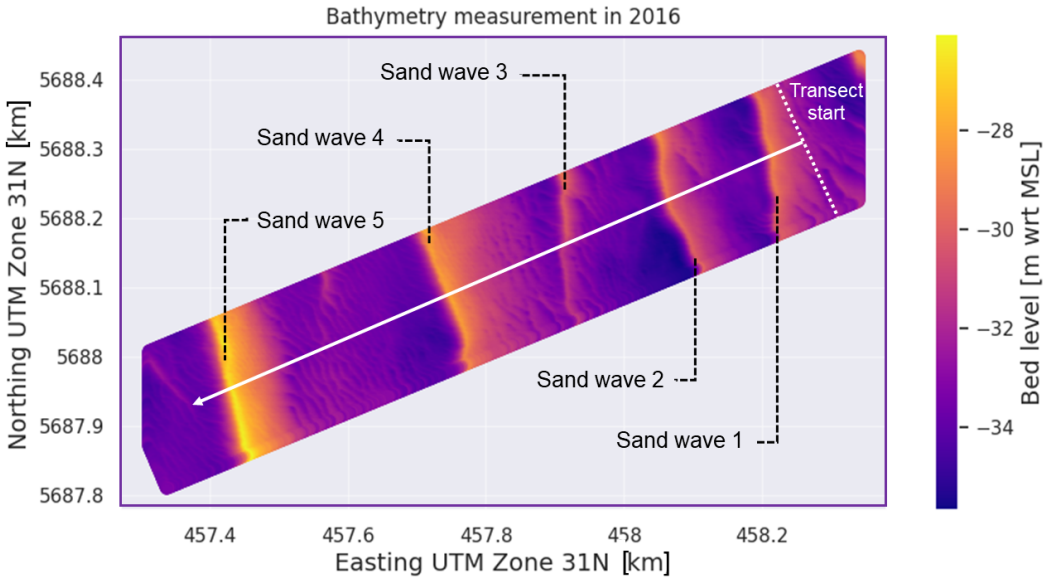

Figure 3.2: Bathymetry measurement of AOI in 2016 and sand wave enumeration.

In the thesis of Tam (2023) an extensive analysis was performed on the bathymetry measurements of the group of sand waves in terms of hydrodynamics, characteristics and behaviour. For further details the reader is referred to the case study chapter of this thesis, however for completeness the most important findings are repeated here.

From the bathymetry records it is found that the sand waves migrate in southwest direction. Each sand wave has a different migration rate, but on average they move 1.4 m per year with a standard deviation of 1.5 m. After dredging the sand waves recovered, but did not always maintain their ridge shape and tails were formed in some of the sand waves. In the area near the dredged trench, sand wave heights were influenced by the recovery processes of the sand waves in the trench. The elevation of the sand waves in the vicinity of the trench dropped with 1-3 m after dredging. This influence could be observed up to 100 m on each side of the trench. The bathymetries of the sand waves in 2018 (just after dredging) and 2021 are shown in Figure 3.3.

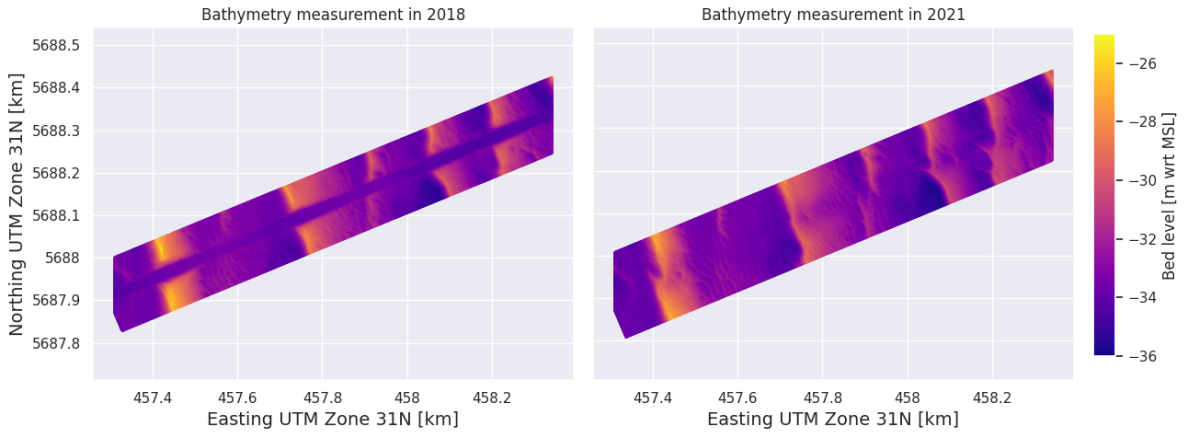

Figure 3.3: Bathymetry measurements of AOI in 2018 (National Grid (UK) and Elia (BE), 2018) and in 2021 (EMODnet, 2021).

A sediment budget analysis is performed on different zones within the trench to see how the sediment is distributed in the years after the trench was dredged. The trench is divided into three zones; a northern zone, a centre zone and a southern zone. These are depicted in Figure 3.4. The zones each have equal surface areas.

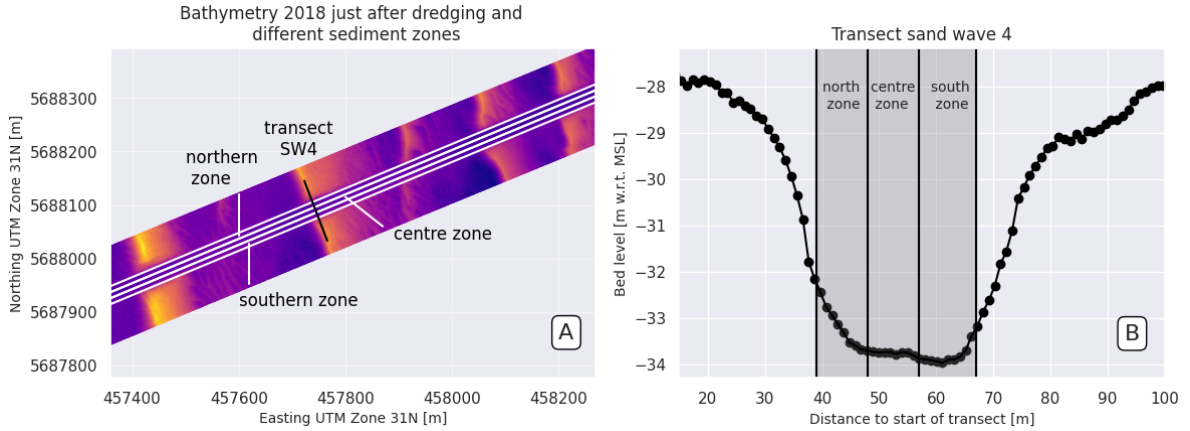

Figure 3.4: Different sediment zones within the trench. In subfigure B the northern zone seem to capture a steeper part of the slope than in the southern zone. This is the case for this transect, but the transects vary along the length of the trench. Overall, an equal steepness on both sides of the trench is captured.

The bathymetry measurement just after the dredging of the trench in 2018 is compared to the bathymetry measurement roughly three years later in 2021 (both depicted in Figure 3.3). Is is found that after three years the sediment budget has increased most in the centre zone compared to the other zones. Moreover, more sediment has entered the southern zone compared to the northern zone. Hence, some sort of asymmetry is observed in the infilling of sediment into the different zones of the trench. Figure 3.5 refers to the exact changes in sediment budget for each of the three zones over the three years.

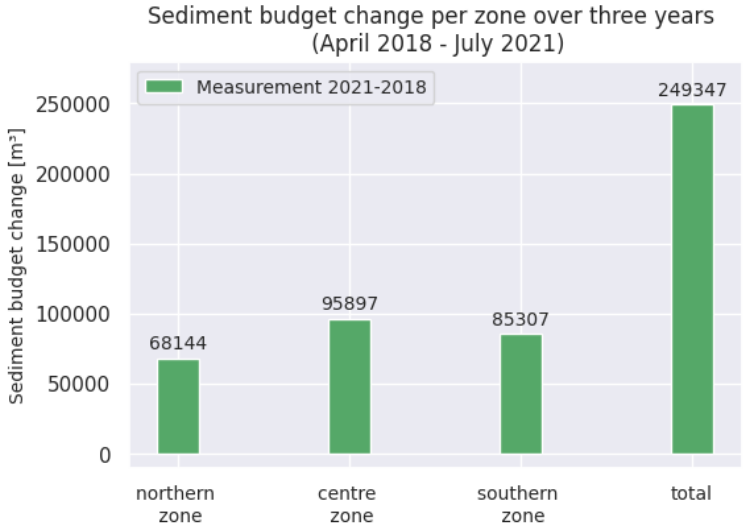

Figure 3.5: Sediment budget change per zone in the trench over a three year period.

3.2. Results analysis of residual currents

3.2.1. Settings DCSM model

In order to retrieve the hydrodynamic conditions at the Area Of Interest, the 3D Dutch Continental Shelf Model - Flexible Mesh (DCSM) is used. The DCSM is a process-based model in Delft3D FM, which uses, amongst others, meteorological forcing to hindcast water levels, currents, sea-temperature and salinity levels over the entire Dutch Continental Shelf. For a complete overview of the settings of this model the reader is referred to the report of Deltares on the validation and setup of the model (Deltares, 2018). The DCSM is run for the period of April 1st 2018 to March 31st of 2021. Four different types of model simulations are run. An overview of the simulations and the settings can be found in Table 3.1.

Simulation	Description and settings
1. All Forcing Mechanisms (AFM)	In this run all forcing mechanisms are included.
2. Only tide (OT)	All forcing mechanisms are turned off, only the tidal forcing is present.
3. No Temperature/Salinity (NTS)	Temperature and salinity calculations are switched off, all other forcing mechanisms are present.
4. No Wind/Atmospheric pressure (NWA)*	Wind and atmospheric pressure are removed as boundary conditions, all other forcing mechanisms are present.

Table 3.1: Overview of DCSM model simulations. * It must be noted that due to computational limitations the desired spin-up period of one calendar year for the salinity and temperature during the simulation which excluded wind and atmospheric pressure (simulation NWA) could not be reached. In light of the results which will be revealed later in this chapter, it was concluded that this deficiency in spin-up time would not affect the final conclusions drawn in this chapter.

The simulations are run for the settings mentioned above, and the values for the water levels, currents, wind velocities, temperature, and salinity are retrieved from the grid cell in the DCSM model that is nearest to the Area Of Interest. This grid cell will from now on be referred to as station 17. The location of station 17 with respect to the Area Of Interest is shown in Figure 3.6. The residual currents in different stations surrounding the Area Of Interest were also investigated, and comparable results are found to those presented in this analysis.

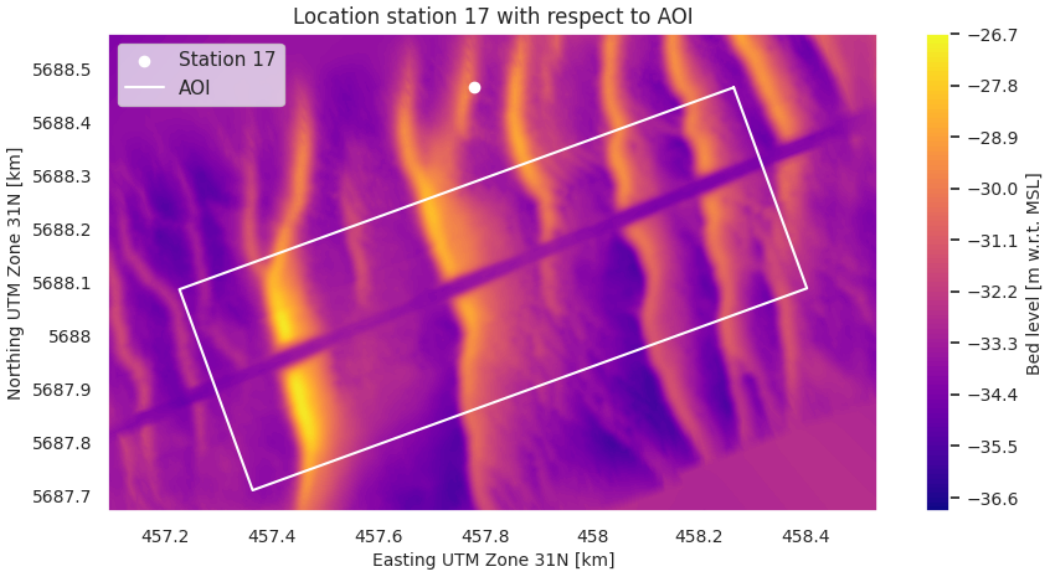

Figure 3.6: Location station 17 with respect to Area Of Interest.

In this analysis, and in the remaining parts of the thesis, it was decided to only display depth-averaged currents. The DCSM model uses a different vertical layer system than the NEMO model, which makes it difficult to compare the velocities near the bed. Analysing the depth-averaged currents also allows for a fair comparison between influences that might be more evident at different heights in the water column, such as the influence of wind and the influence of bed forms.

3.2.2. Characteristics of residual currents

First, the residual currents are studied for the simulation including all forcing mechanisms and the simulation which only includes tidal forcing. In Figure 3.7 the probability density plots are shown for the depth-averaged currents for the entire period at station 17, as well as for the depth-averaged tidal currents, and the depth-averaged residual currents. The depth-averaged residual currents are calculated by subtracting the depth-averaged tidal currents (from the simulation which only includes tidal forcing) from the total depth-averaged currents (from the simulation which includes all forcing mechanisms).

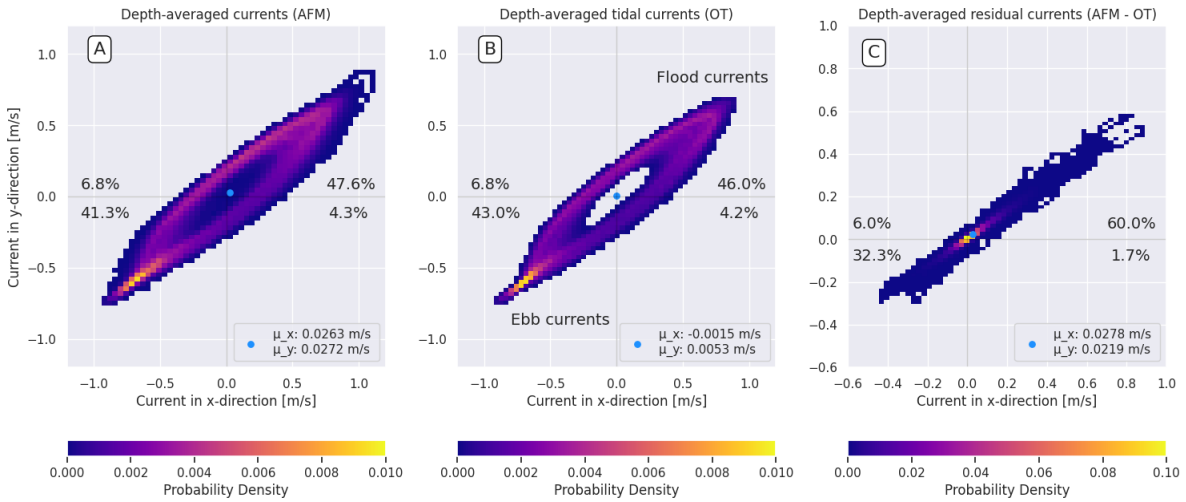

Figure 3.7: Probability density plots of depth-averaged currents at Station 17. The blue dots indicate the time-averaged mean of the depth-averaged currents in both directions at station 17 per simulation. A: simulation which includes all forcing mechanisms (AFM). B: simulation which includes only tidal forcing (simulation OT). C: depth-averaged residual currents, currents from simulation which includes all forcing mechanisms minus currents from simulation which only includes tidal forcing (simulation AFM - simulation OT).

The depth-averaged tidal currents flow along two axes; the flood currents are directed towards the northeast (53°N), and ebb currents are directed towards the southwest (233°N). The time-averaged depth-averaged tidal currents are close to zero, indicating that the flood and ebb currents balance each other. The depth-averaged tidal currents show magnitudes ranging from 0.07 m/s to 1.18 m/s. When examining the depth-averaged residual currents, the flow is directed along two axes similar to the orientation of the tidal axes. The majority of the time (60%) the residual currents are pointed towards the northeast, and the time-averaged depth-averaged residual currents are also pointed in this direction. The maximum residual currents in northeast direction are also higher than the maximum residual currents pointed towards the southwest. Hence, a clear dominance of the depth-averaged residual currents towards the northeast is observed. The depth-averaged residual currents show magnitudes ranging from 0 to 1 m/s, of which 85% is below 0.15 m/s. This dominance in residual currents exerts its influence on the total depth-averaged currents displayed in subfigure A of Figure 3.7. Whereas the time-averaged depth-averaged tidal currents roughly cancel each other in flood and ebb direction, the residual currents ensure that the time-averaged depth-averaged total currents are shifted towards the northeast. The influence of the residual currents on the total currents is not large when comparing it to the currents generated by the tide. This confirms the statement that the system is tide-dominated.

3.2.3. Event-driven and representative residual currents

In order to learn more about the characteristics of the residual currents a distinction is made based on their magnitudes. The characteristics of the depth-averaged residual currents that belong to the highest five percent in terms of magnitude are compared to the characteristics of the remaining (lowest) residual currents. The highest residual currents are referred to as event-driven residual currents, and the remaining as representative residual currents. The probability density plots of these residual currents are shown in Figure 3.8.

When looking at the depth-averaged representative residual currents the characteristics of the distribution are not affected rigorously. The majority of the residual currents is still directed towards the northeast, and overall the time-averaged depth-averaged residual currents are still pointed in the same direction, however the magnitude has decreased. For the highest depth-averaged residual currents the dominance towards northeast has become even stronger. Now 84% of the currents are directed towards the northeast, and the time-averaged depth-averaged magnitudes have increased significantly.

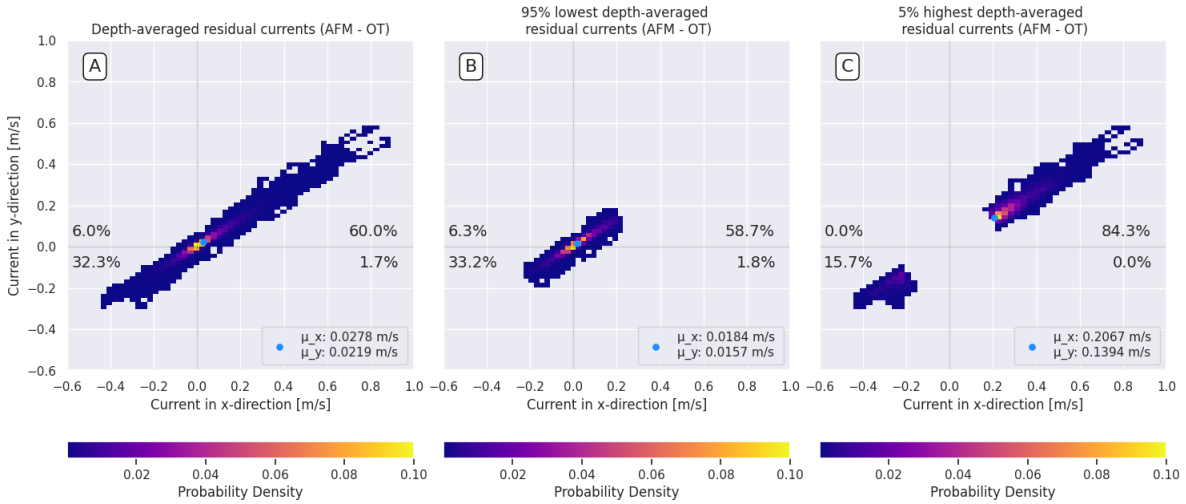

Figure 3.8: Probability density plots of depth-averaged residual currents at station 17. A: Depth-averaged residual currents which occur 100% of the time. B: The 95% of the remaining depth-averaged residual currents. C: The 5% of the highest depth-averaged residual currents.

3.2.4. Forcing mechanisms behind residual currents

In order to unravel which forcing mechanisms are responsible for the generation of the residual currents in the Area Of Interest the residual currents of the simulation without temperature and salinity and the simulation without wind and atmospheric pressure are compared to the residual currents of the simulation which includes all forcing mechanisms. The residual currents are computed in the same way as before; the depth-averaged currents of the simulation which only includes tidal forcing is subtracted from the depth-averaged currents from the simulation in question. The effects of the exclusion of salinity and temperature calculations are shown in Figure 3.9, and the effects of excluding wind and atmospheric pressure forcing are depicted in Figure 3.10.

In subfigure A of Figure 3.9 the depth-averaged residual currents are shown for the entire three-year period for the simulation which includes all forcing mechanisms and the simulation which excludes temperature and salinity. By visual inspection it becomes obvious that the depth-averaged residual currents (here only shown in x-direction, but in y-direction the results look similar) do not differ that much between the two simulations. When quantitatively assessing the data, as is done in subfigure C and D, a very high Pearson correlation coefficient is found, which indicates a high correlation between the depth-averaged residual currents of the two simulations. On top of this, a root mean square error is found which is in the order of magnitude of roughly 0.01 m/s. The positive mean average error indicates that the velocities during the simulation with all forcing mechanisms are on average higher than those of the simulation without salinity and temperature, which can also be observed upon visual inspection. The exclusion of salinity and temperature does not seem to influence the residual currents significantly.

When looking at the effects of excluding wind and atmospheric pressure a different result is obtained. Again subfigure A of Figure 3.10 shows the depth-averaged residual currents for the entire three-year period for both simulations. The depth-averaged residual currents (in x-direction, again the results are similar in y-direction) from the simulation which excludes wind and atmospheric pressure looks completely different from the simulation which includes all forcing mechanisms. Subfigure C and D assess the relationship between the depth-averaged residual currents quantitatively, and here a very low correlation coefficient is found, indicating a very weak relationship between the two variables. The root mean square error is in the order of magnitude of 0.06-0.09 m/s for both x and y direction respectively, which is very high compared to the magnitudes of the residual currents from the simulation which includes all forcing mechanisms. Hence, wind and atmospheric pressure forcing are the main drivers behind the residual currents shown in the Area Of Interest.

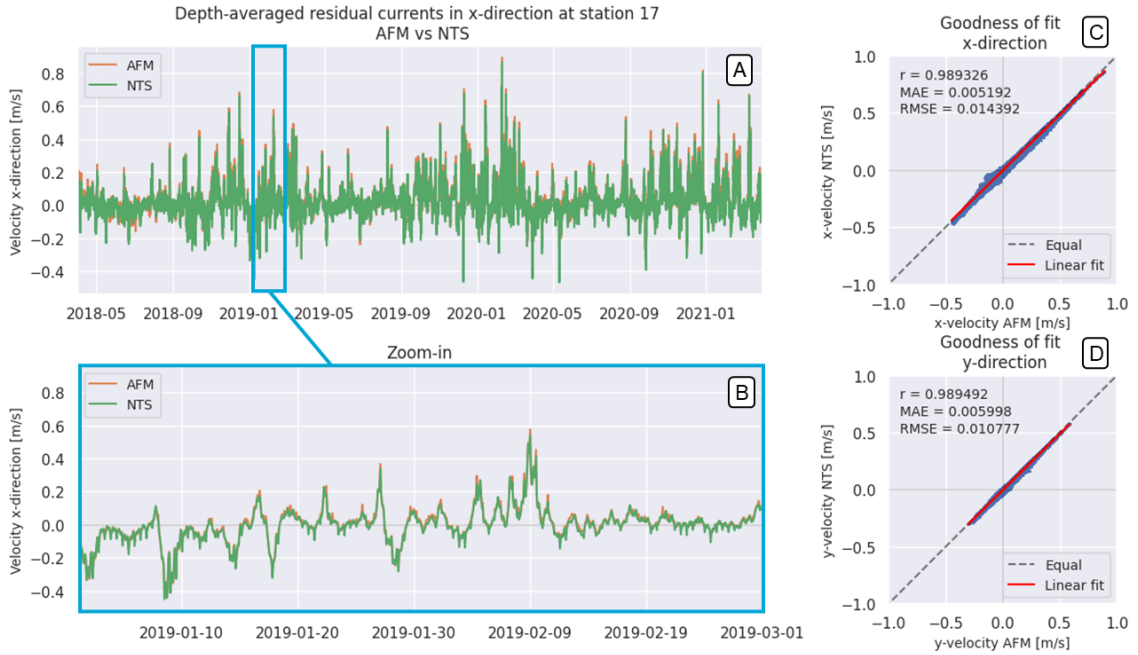

Figure 3.9: A comparison between depth-averaged residual currents of the simulations which includes all forcing mechanisms (AFM) and which excludes temperature and salinity (NTS). C&D: Goodness of fit between the depth-averaged residual currents in both directions, r: Pearson correlation coefficient, MAE: mean average error, RMSE: root mean square error.

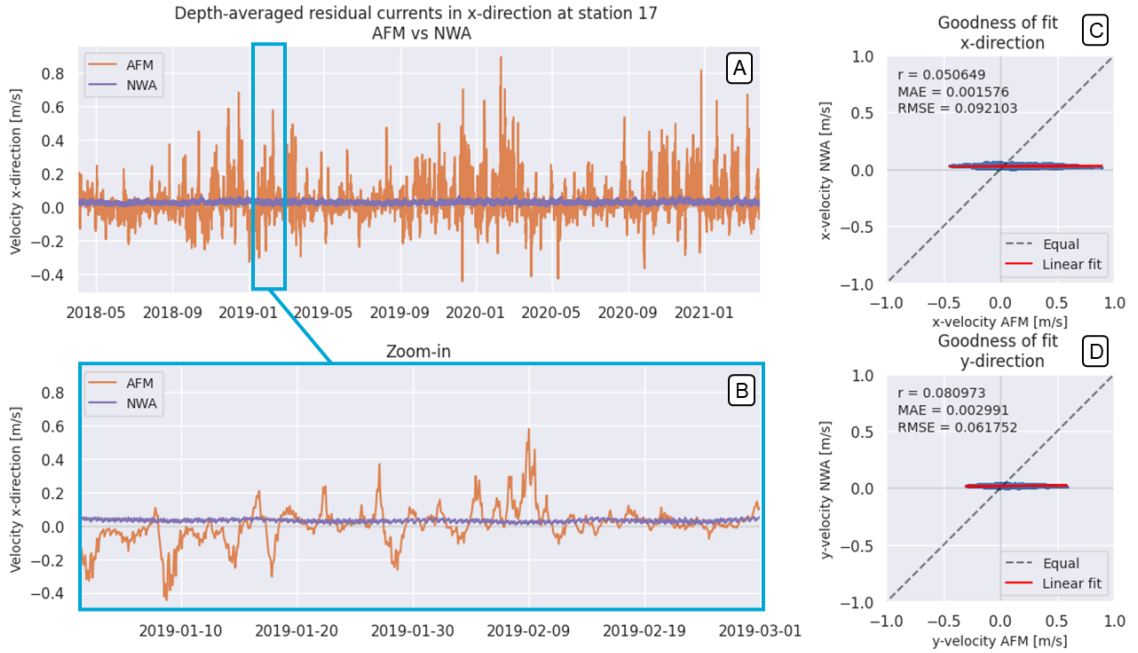

Figure 3.10: A comparison between depth-averaged residual currents of the simulations which includes all forcing mechanisms (AFM) and which excludes wind and atmospheric pressure (NWA). C&D: Goodness of fit between the depth-averaged residual currents in both directions, r: Pearson correlation coefficient, MAE: mean average error, RMSE: root mean square error.

4

Numerical Modelling

In order to examine the effects of the residual currents studied in the previous chapter on the morphological interactions between sand waves and trenches, the case study is translated into a numerical model in Delft3D FM. The settings of this model are discussed first, which is followed by a description of the modelling scenarios. Next, the performance of the nesting of the boundary conditions is tested. Finally, the results are shown for the short- and intermediate-term modelling scenarios.

4.1. Model Settings

The model used in this thesis was developed in the thesis of Tam (2023). Hence, the reader is referred to this thesis for a complete and detailed overview of the model settings and validation. However, the most important settings are repeated here, as well as the model adaptations done to improve the model.

4.1.1. Computational grid and vertical discretisation

The computational grid is rectangular and consists of smaller nested grids. The grid is roughly 3500m in the longitudinal direction and 4500m in the transverse direction. The grid cell size decreases from 128 m by 320 m at the edges until it has reached a configuration of 2m by 5m in the most detailed part of the grid, which coincides with the Area Of Interest. The centreline of the trench roughly aligns with the longitudinal orientation of the Area Of Interest. Figure 4.1 refers to the overall composition of the grid. For vertical discretisation, a sigma-coordinate system is used. Contrary to the thesis of Tam (2023) 30 grid cells are used in vertical direction instead of 40. This was done to reduce computational time. The grid size in vertical direction begins with a height of 0.075% of the water column and increases on a logarithmic scale until it reaches the water surface.

4.1.2. Boundary conditions

Water level and advection boundary conditions are used to impose the hydrodynamic conditions of the DCSM on the model domain. This type of boundary condition requires two types of input; water level time-series and time-series of the velocity profiles in two horizontal directions. These time-series are extracted from different locations of the DCSM and applied to the nearest locations of boundary condition points in the model.

In the previous chapter it was observed that wind is among the forcing mechanisms that are largely responsible for the generation of the residual currents. For this reason, some model tests were done which included wind as boundary condition. It was found that the inclusion of wind did not cause any significant effects on the hydro- and morphodynamics of the model. Therefore it was decided to exclude the wind forcing in the model simulations performed in this chapter. In the previous chapter it was also found that salinity and temperature do not play a large role in the generation of residual currents in the Area Of Interest, hence these are also excluded from the model simulations.

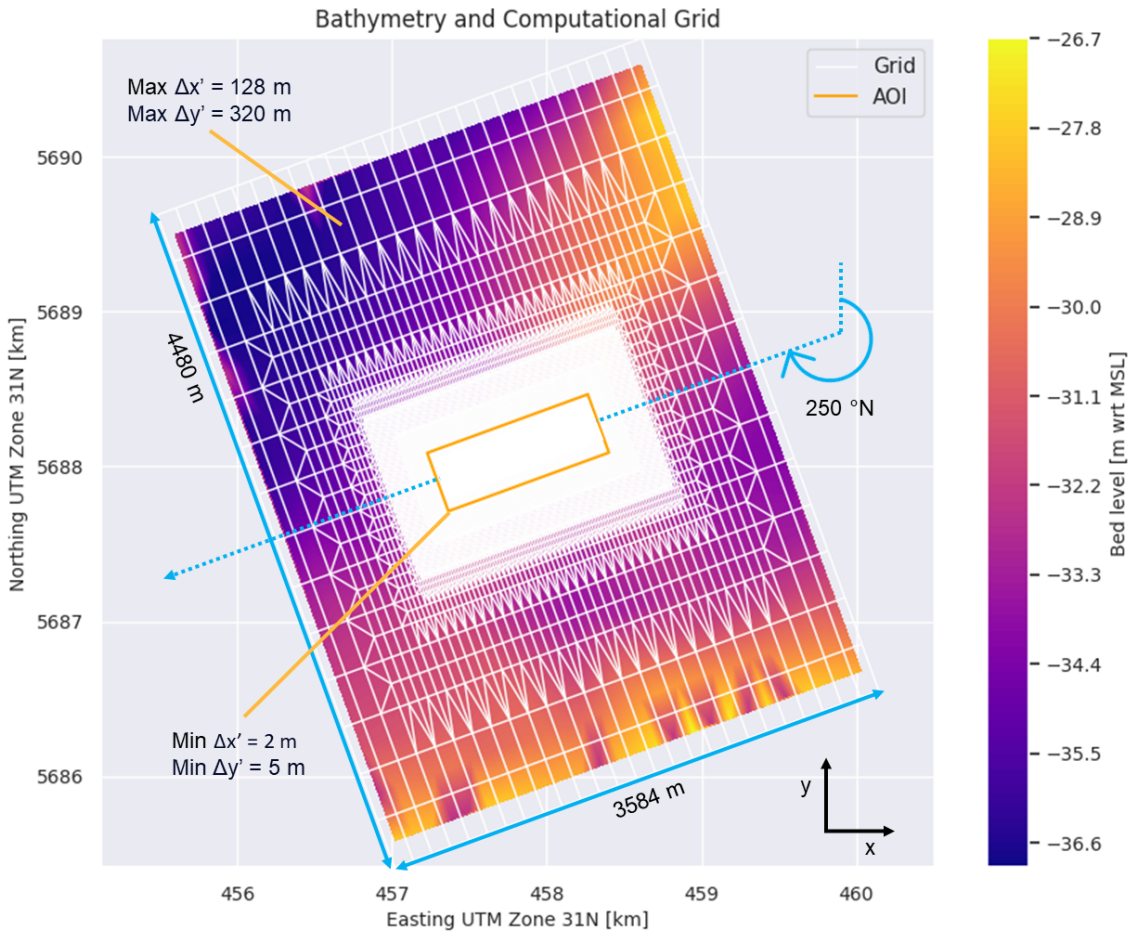

Figure 4.1: The model domain.

4.1.3. Bathymetry

The model bathymetry consists of two merged bathymetry datasets. The first dataset is the bathymetry measurement of April 2018 which was conducted just after the trench was dredged. These measurements were provided by the Nemo Link project and have a resolution of 1m x 1m. This dataset is confined to the trench area and therefore does not extend much beyond the Area Of Interest. Hence it was decided to make use of a second dataset, which is the bathymetry that is also used in the DCSM. This dataset has a much lower resolution (roughly 840m to 930m) but extends well beyond the Area Of Interest. The first dataset is placed within the second dataset, and at the interface between the two datasets the bathymetry is smoothened to ensure a fluent transition.

Using this bathymetry as a starting point of the simulations led to initial dampening of smaller scale features which cannot be resolved due to limited model resolution, and some adaptations in sand wave shape. In order to limit the influence of these spin-up effects it was decided to run the initial bathymetry for a month under calm hydrodynamic conditions, resulting in a smoothened bathymetry. The smoothened bathymetry of this run was then used as a starting point for all of the simulations that are done in this chapter.

4.1.4. Sediment parameters and transport formulation

Van Rijn (2007) is used as the sediment transport formulation, this is in line with the publication of Overes et al. (2024) which considers the effects of time-varying residual currents on sand wave systems and the thesis by Choy (2015) on the effects of sediment transport formulations on sand wave dynamics. The sediment formulation is used in combination with the bed slope transport formulation by Bagnold (1966) for the longitudinal slope and Ikeda (1982, 1988) for transverse slopes. Default settings were

used for the streamwise and transverse bed slope parameters (α_{bs} = 1.0 and α_{bn} = 1.5). For a more detailed description of the sediment transport formulations the reader is referred to the User Manual on D-Morphology (Deltares, 2024). A morphological spin-up time of two tidal cycles is used (24.84 hours), after which the bed level update is switched on. Similar to the thesis of Tam (2023) the bed material is non-cohesive sediment with a median grain size diameter (d_{50}) of 350 µm, which is based on measurements and a sensitivity analysis. Suspended load transport is considered to be beyond the scope of the thesis, hence only bed load transport is included in the model.

4.1.5. Overview model settings

In Table 4.1 an overview of all the model settings can be found, the asterisk indicates that the settings have changed with respect to the model in the thesis of Tam (2023).

Model settings	
Grid size in AOI	2m x 5m
Number of vertical layers*	30
Type of boundary conditions	Water level and advection velocity
Wind forcing	No
Salinity	No
Temperature	No
Bathymetry*	Composite bathymetry which is smoothened for one month
Sediment transport formulation*	Van Rijn (2007)
Streamwise bed slope factor*	1
Transverse bed slope factor	1.5
Morfac*	1
Spin-up time*	24.84h
Median sediment diameter	350 µm
Bed load transport	Yes
Suspended load transport	No

Table 4.1: Overview model settings. *These settings have been adapted with respect to the model presented in Tam (2023).

4.2. Modelling scenarios

In section 3.2.3 a distinction is made between event-driven residual currents (the highest residual currents in terms of magnitude which occur 5% of the time) and residual currents during representative hydrodynamic conditions (the remaining 95% of the residual currents). To be able to study the effects of residual currents on the morphological interactions between sand waves and trenches thoroughly it was decided to focus on two modelling scenarios. One which focuses on event-driven residual currents, and the other which focuses on residual currents during representative hydrodynamic conditions. Both modelling scenarios are associated with their own timescales. The event-driven residual currents are studied over the coarse of a few tidal cycles, hence referred to as the “short-term” scenario, and the representative residual currents are studied for one spring-neap tidal cycle (28 tidal cycles) and is hence referred to as the “intermediate-term” scenario.

4.2.1. Scenario 1: Short-term

The highest residual currents that were observed in the Area Of Interest over the course of the three year period occurred on the 9th of February in 2020. The high values can be attributed to the storm Ciara which passed the Area Of Interest during that period (KMI, 2020). The residual currents showed magnitudes up to 1.03 m/s during the peak of the storm, and were pointed towards the northeast. Storm Ciara exerted its influence on the residual currents for approximately three full tidal cycles. Storm Ciara occurs during a moment in time in which the tide has almost reached its maximum tidal amplitude during spring tide. Figure 4.2 refers to the timing of storm Ciara with respect to the tide in the context of one year.

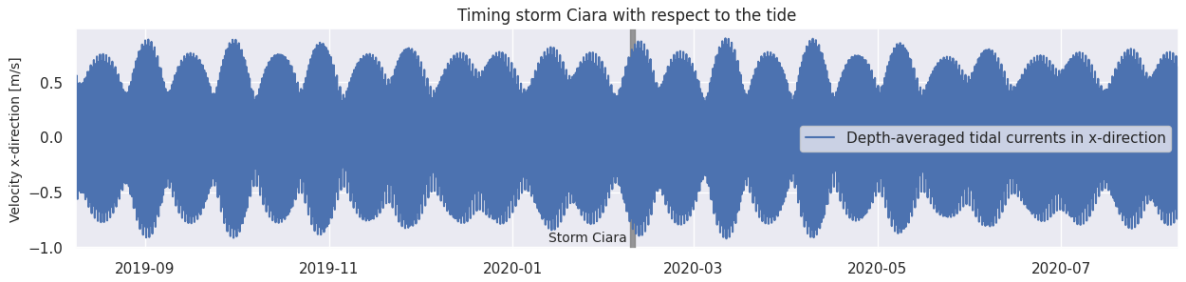

Figure 4.2: Timing storm Ciara with respect to the tide.

4.2.2. Scenario 2: Intermediate-term

A period of 28 tidal cycles, one spring-neap tidal cycle, is selected in which the distribution of the residual currents resembles the distribution of the residual currents in 95% of the time over the period of 2018-2021. The distribution of the residual currents in 95% of the time is shown on the left in Figure 4.3 and for the selected period (15th of October 2019 to the 29th of October 2019) on the right.

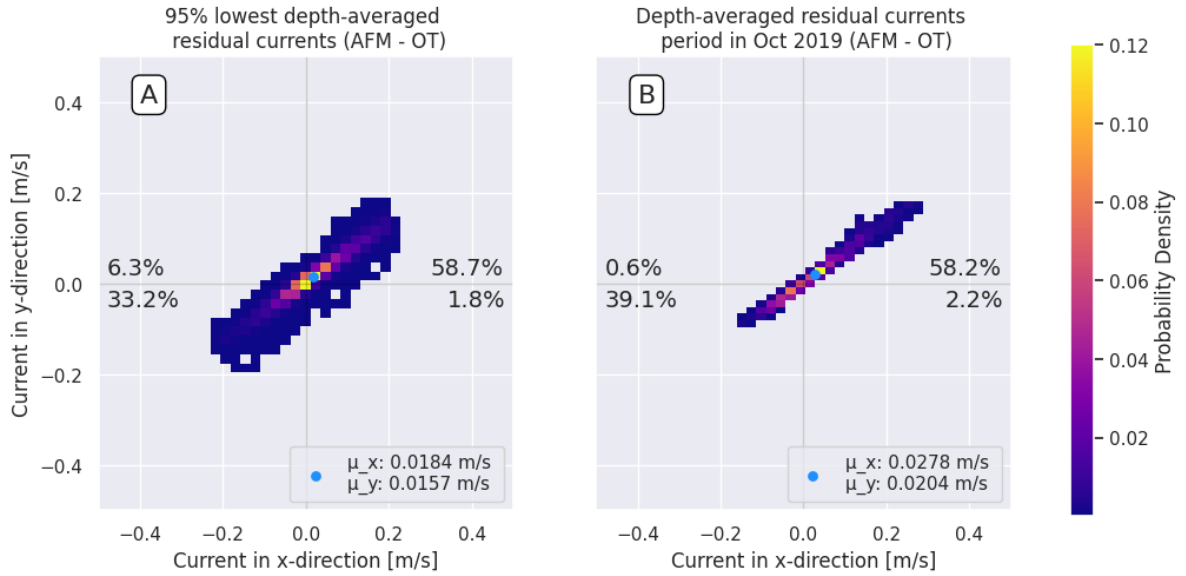

Figure 4.3: A. Probability density plots for the lowest 95% of the residual currents. B. Probability density plot for the residual currents during the period of October 15th 2019 to October 29th 2019.

The percentage of residual currents directed towards the northeast in the fourteen day period is roughly the same as for the three-year period. In southwest direction, there is an increase in percentage of residual currents considering the fourteen day period. Additionally, the time-averaged depth-averaged residual currents are still pointed towards the northeast, however an increase in magnitude is observed for the fourteen day period. Overall, these changes in characteristics are considered small, and the selected period is able to capture the characteristics over a three-year period well in fourteen days.

4.3. Hydrodynamic performance of nesting

There are no hydrodynamic measurements available in the Area Of Interest to which the model can be validated. It is however possible to compare the hydrodynamic conditions at station 17 of the NEMO model to the hydrodynamic conditions of the DCSM model to test the nesting. In Figure 4.4 the results of this comparison are shown for the intermediate-term modelling, the results of the short-term modelling are similar and are not displayed here in view of brevity.

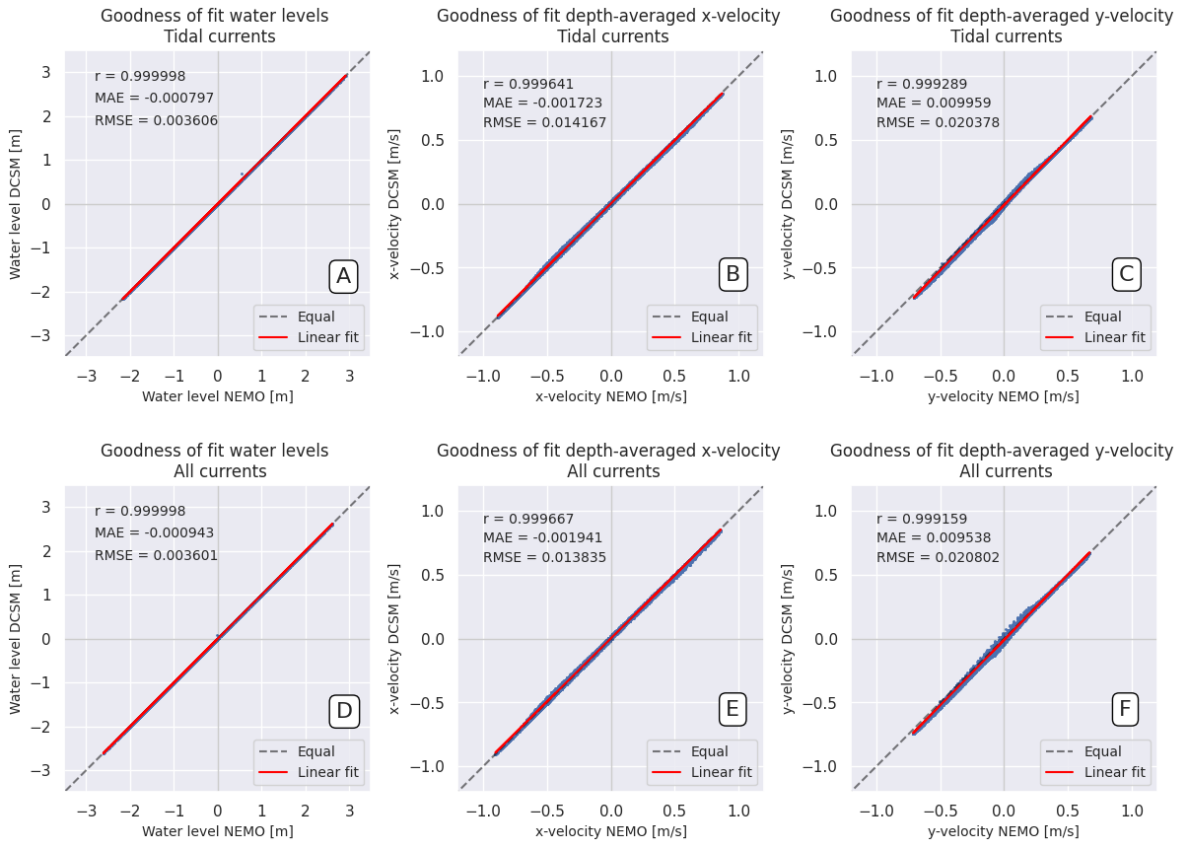

Figure 4.4: Goodness of fit per water level (A and D), depth-averaged x-velocity (B and E) and depth-averaged y-velocity (C and F) at station 17, for the intermediate-term simulation which only includes tidal forcing and for the intermediate-term simulation which includes all forcing.

A good match is found between the water levels and depth-averaged velocities in the NEMO model and the DCSM. The root mean square errors are very low compared to the order of magnitudes of the water levels and depth-averaged velocities. The root mean square error does however increase slightly when looking at the velocities in y-direction, where more scatter can be observed near the zero velocities. This is an indication that the NEMO model is less accurate in replicating the hydrodynamics in that direction. When looking at sand wave systems it is however more important that the highest velocities are reproduced well, as higher velocities induce more morphological change (see Figure 1.3). Based on this, and considering the order of magnitudes it is concluded that the nesting of the hydrodynamic conditions went successfully.

4.4. Modelling results

4.4.1. Short-term: Hydrodynamic differences

First the differences in flow velocities are compared for the simulation which only includes tidal forcing and for the simulation which includes all currents. In doing so, the velocities are retrieved from the NEMO model and averaged over the depth and horizontal. The grid cells used in horizontal direction are shown in Figure 4.5. The depth and horizontally averaged velocity in x-direction is shown in subfigure A of Figure 4.6. The depth-averaged velocities strongly increase in the Area Of Interest in x-direction during storm Ciara. The increase in y-direction is similar, and hence not shown here in view of conciseness. Subfigure B and C in Figure 4.6 shows that the residual currents ensure a transition towards the northeast direction when considering the velocities in x and y direction.

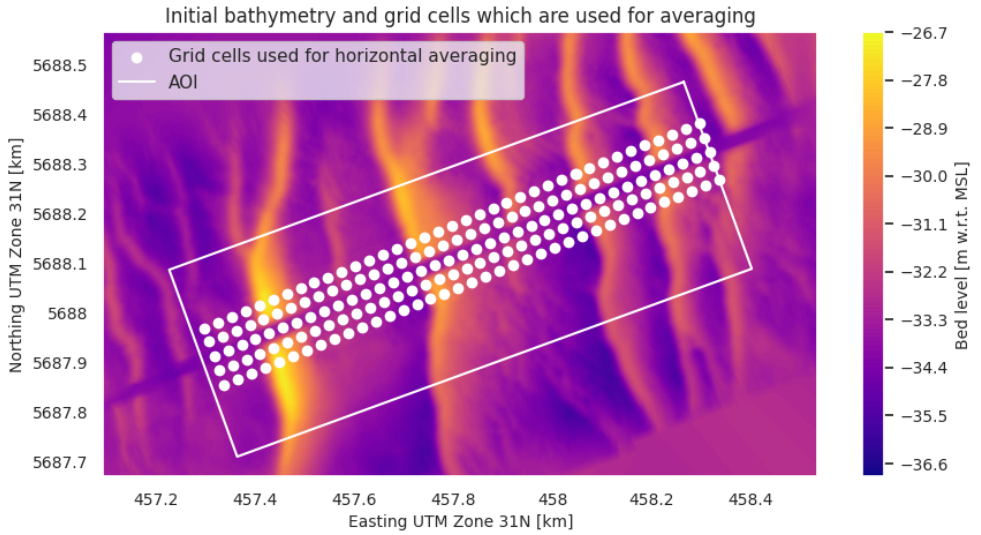

Figure 4.5: Grid cells which are used for horizontal averaging over the Area Of Interest.

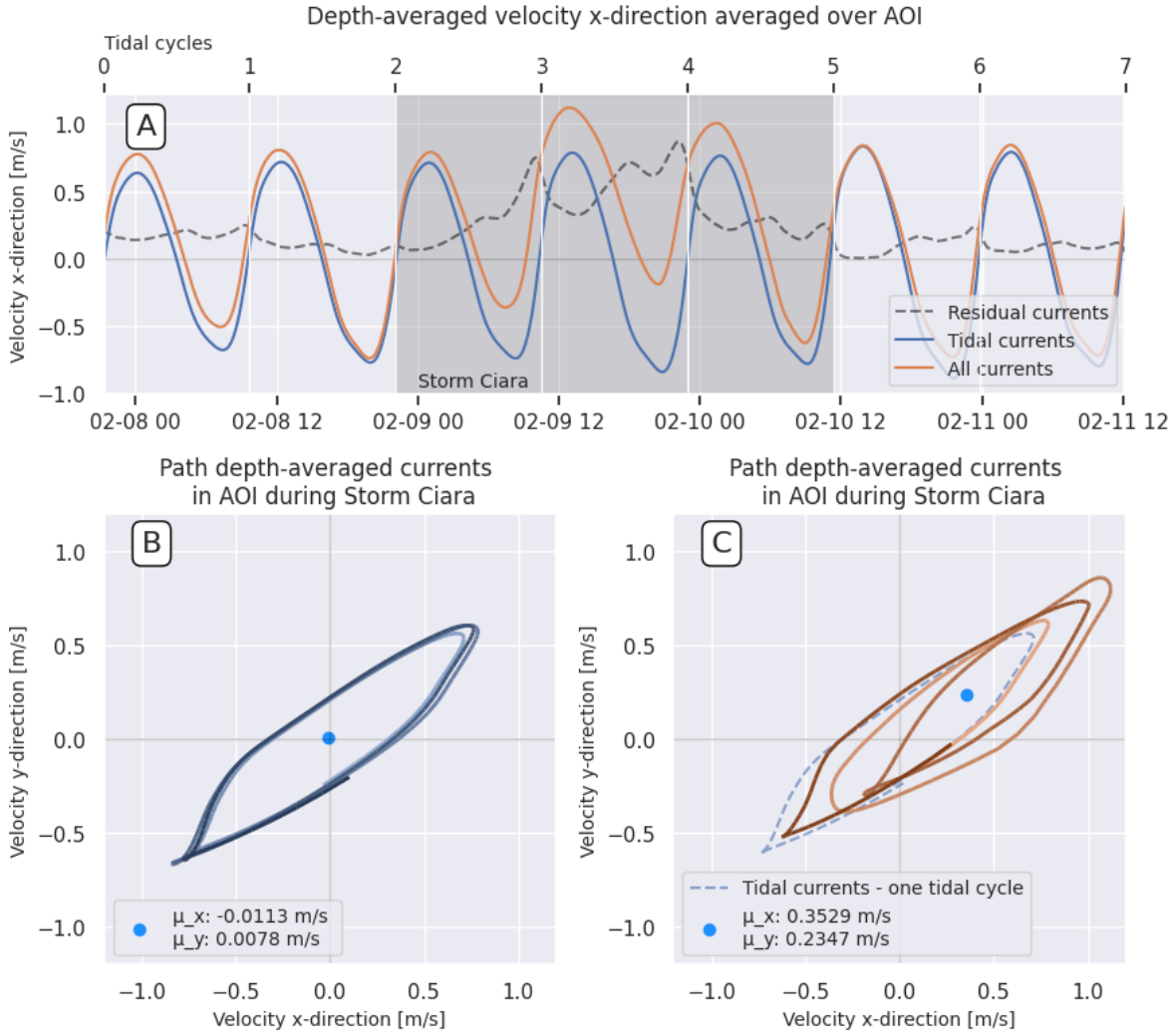

Figure 4.6: Differences in flow velocities between the two simulations. A darker colour of the plot in subfigure B and C indicates the velocity occurred later in time.

4.4.2. Short-term: Morphological differences

Sediment transport scales non-linearly with flow velocity, and occurs only when the shear stress near the bed reaches a critical value (when the velocities are high enough). The increase in flow velocities during storm Ciara ensure a tripling in sediment transport rates towards the northeast during peak flood flow. In southwest direction, the critical value for sediment transport is hardly reached and less sediment is transported in that direction. The sediment transport rates during storm Ciara for both simulations is shown in Figure 4.7.

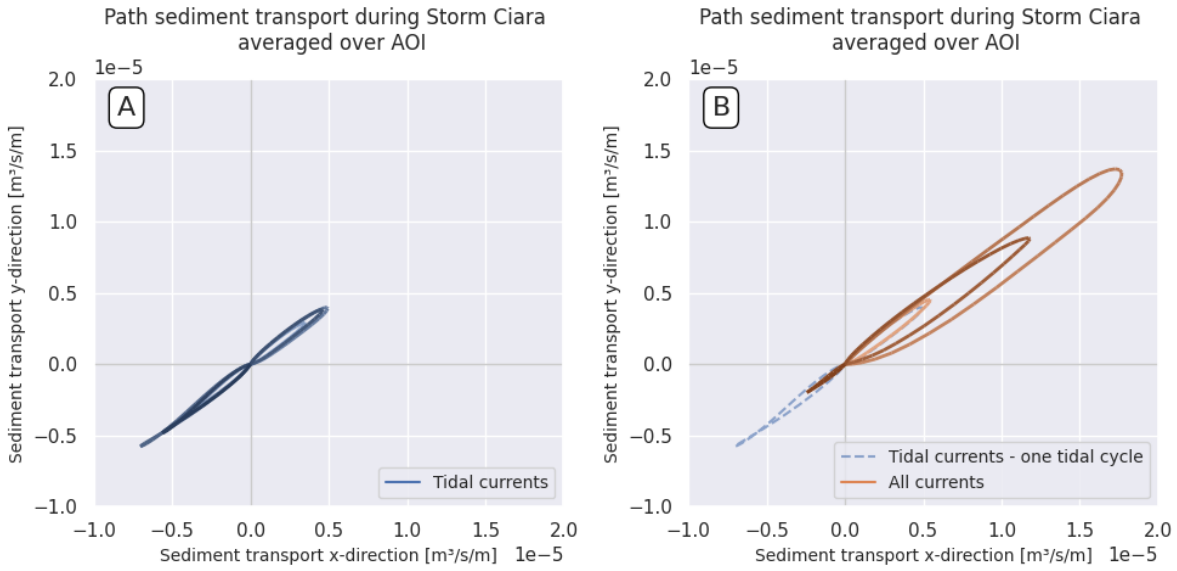

Figure 4.7: Path sediment transport averaged over the Area Of Interest during storm Ciara. The darker the shade of the plot, the later in time the sediment transport occurs.

These changes in flow velocities and sediment transport rates affect the morphological evolution of the seabed. In the simulation which only includes tidal forcing, the time- and space-averaged sediment transport rates are slightly asymmetric and pointed towards the southwest. This ensures that over the entire Area Of Interest erosion takes place at the crest of the sand waves and sedimentation occurs on the steep slopes of the sand waves, this is depicted in Figure 4.8A. The steep slopes of the sand wave refer to the slopes to the southwest of the sand waves, these are steeper compared to the slopes to the northeast of the crests which are more gentle. The residual currents during storm Ciara are able to reverse these sediment transport patterns and cause erosion to occur on the steep slopes of the sand waves and deposition on the gentle slopes, as depicted in Figure 4.8B. Zooming in on a longitudinal transect through the sand waves to the south of the trench (location of transect is depicted in Figure 4.9) confirms the statement that the residual currents cause a reversal in sediment transport patterns. Figure 4.10C shows the relative influence of the residual currents; more deposition on the gentle slopes and more erosion of the steep slopes. The sediment that is deposited at the troughs of the steep slopes of the sand waves during tide-only conditions originates from the crests of the sand waves, this can be observed by looking at the cumulative sediment transport vectors in Figure 4.11A. The sediment transport magnitudes are much higher in the simulation which includes all currents. The sediment transport is directed towards the northeast during storm Ciara and therefore enters the trench under a different angle, as is shown in Figure 4.11B.

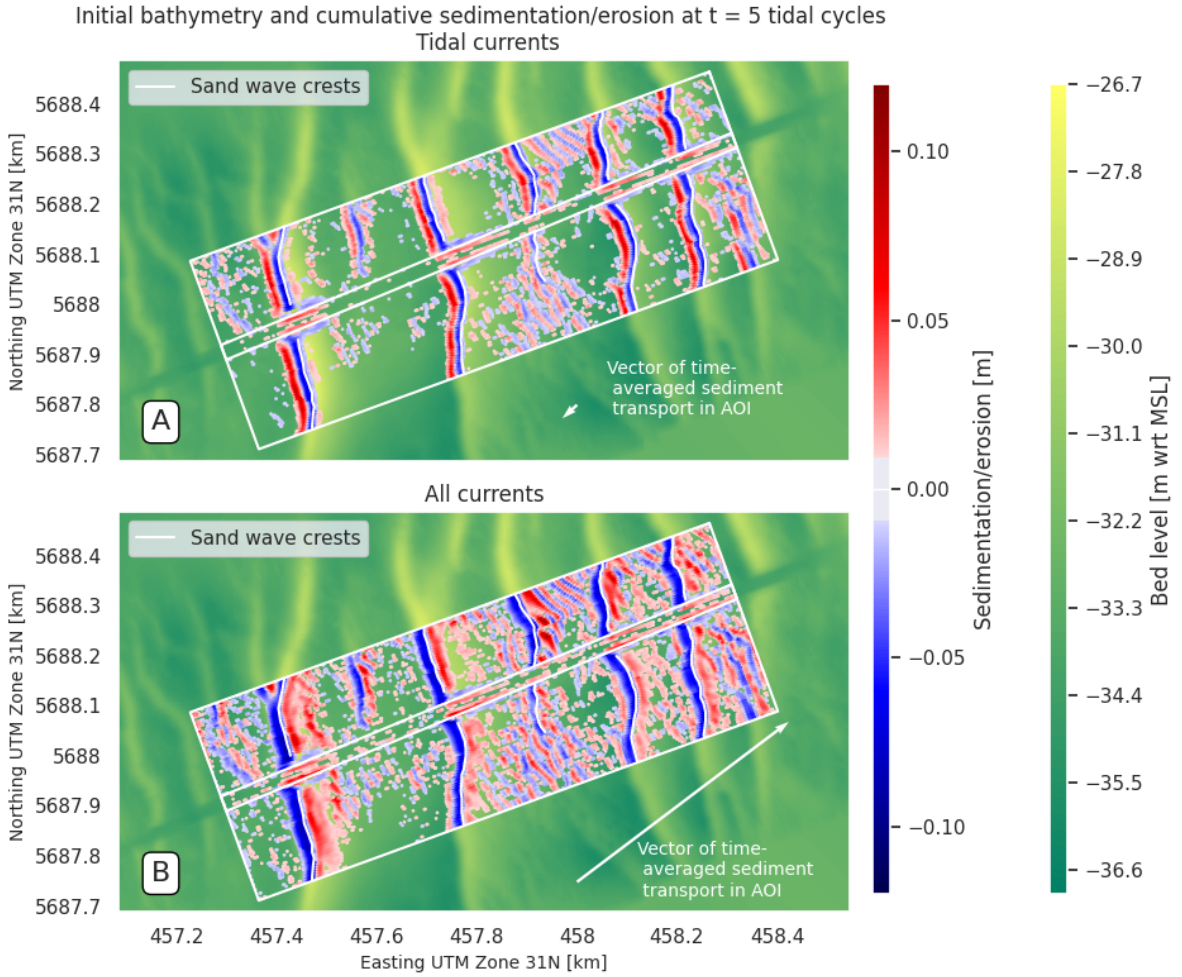

Figure 4.8: Cumulative sedimentation and erosion patterns during storm Ciara.

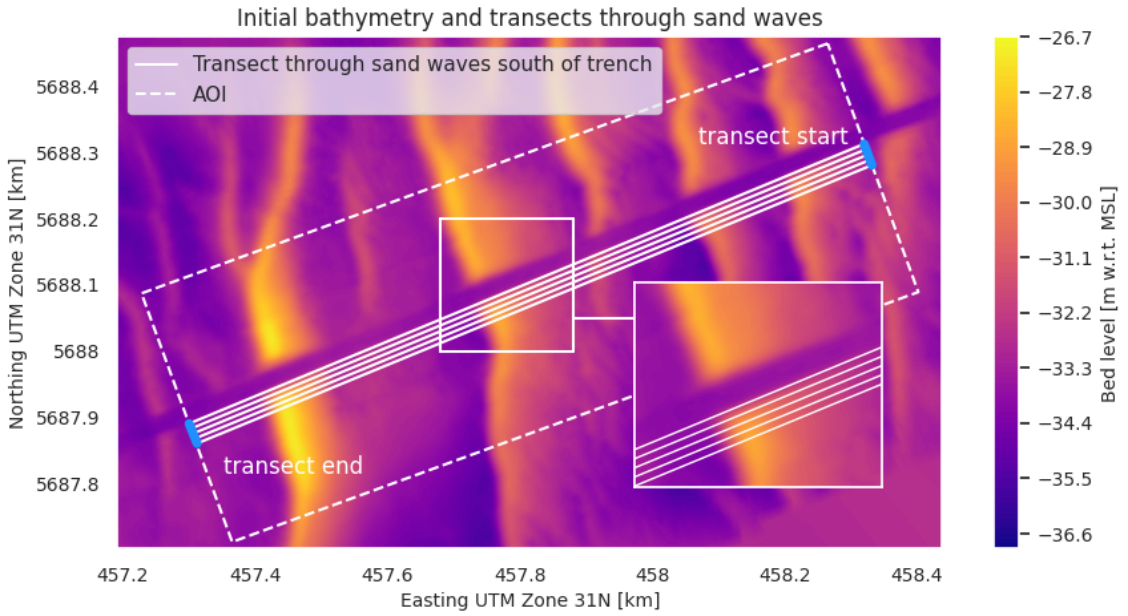

Figure 4.9: Transects of sand waves to the south of the trench.

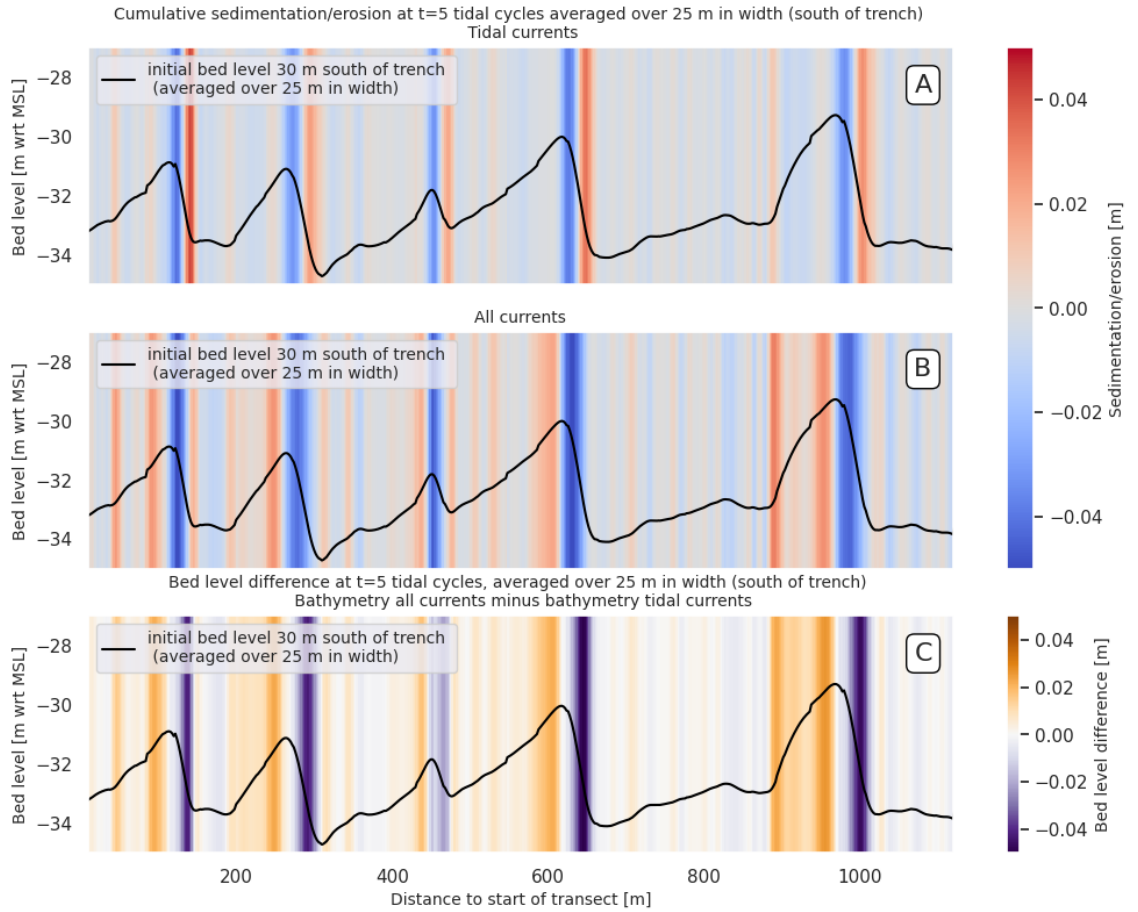

Figure 4.10: A,B: Sedimentation and erosion at the five transects depicted in Figure 4.9 averaged in width to one bed level. C: Final bed level difference between the five transects averaged in width to one bed level. The small jumps in the initial bed level can be attributed to the fact that the grid cells do not entirely align with the transect of the sand waves. Hence small jumps are observed at the locations where the grid cells switch.

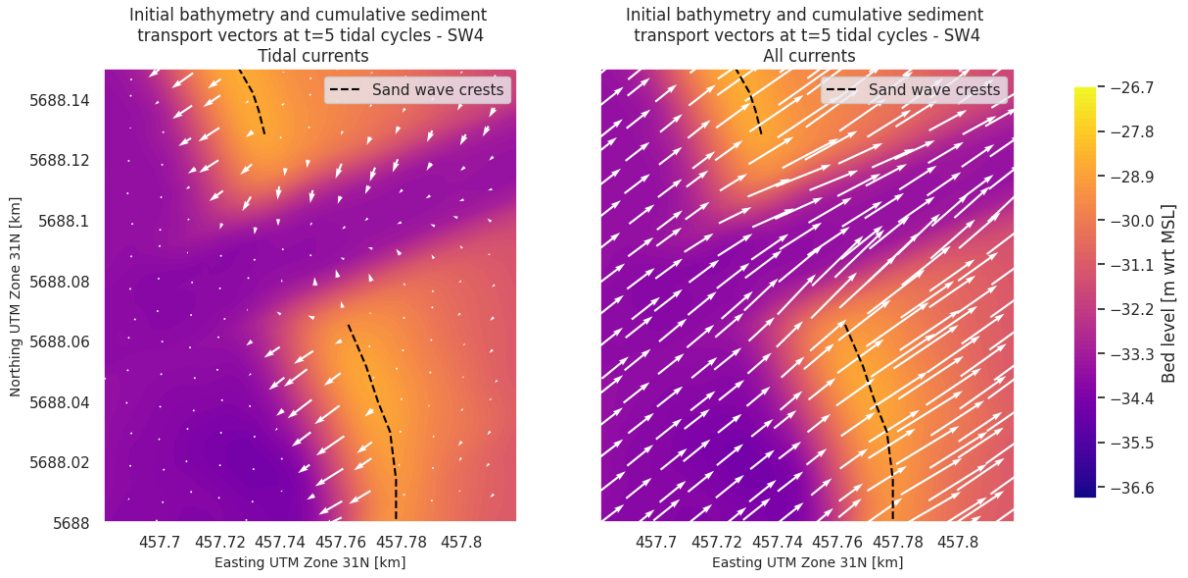

Figure 4.11: Cumulative sediment transport vectors after storm Ciara for sand wave 4 (enumeration defined in Figure 3.2) per simulation. The sediment transport patterns of the other sand waves look similar.

Morphodynamic behaviour within trench

When focusing on the trench, a substantial amount of sedimentation is observed near the sand wave crests in both simulations. During tide-only conditions the southern and northern side of the trench seem to have an equal amount of sedimentation. In the simulation which includes residual currents the southern side seems to be dominant in terms of sediment infilling into trench, this can be observed in Figure 4.12A and B. The imbalance in sedimentation locations in the trench is best visible in Figure 4.12C which shows the bed level difference in the trench between the two simulations after five tidal cycles. The sedimentation levels are lower on the northern side due to the residual currents, and higher on the southern side.

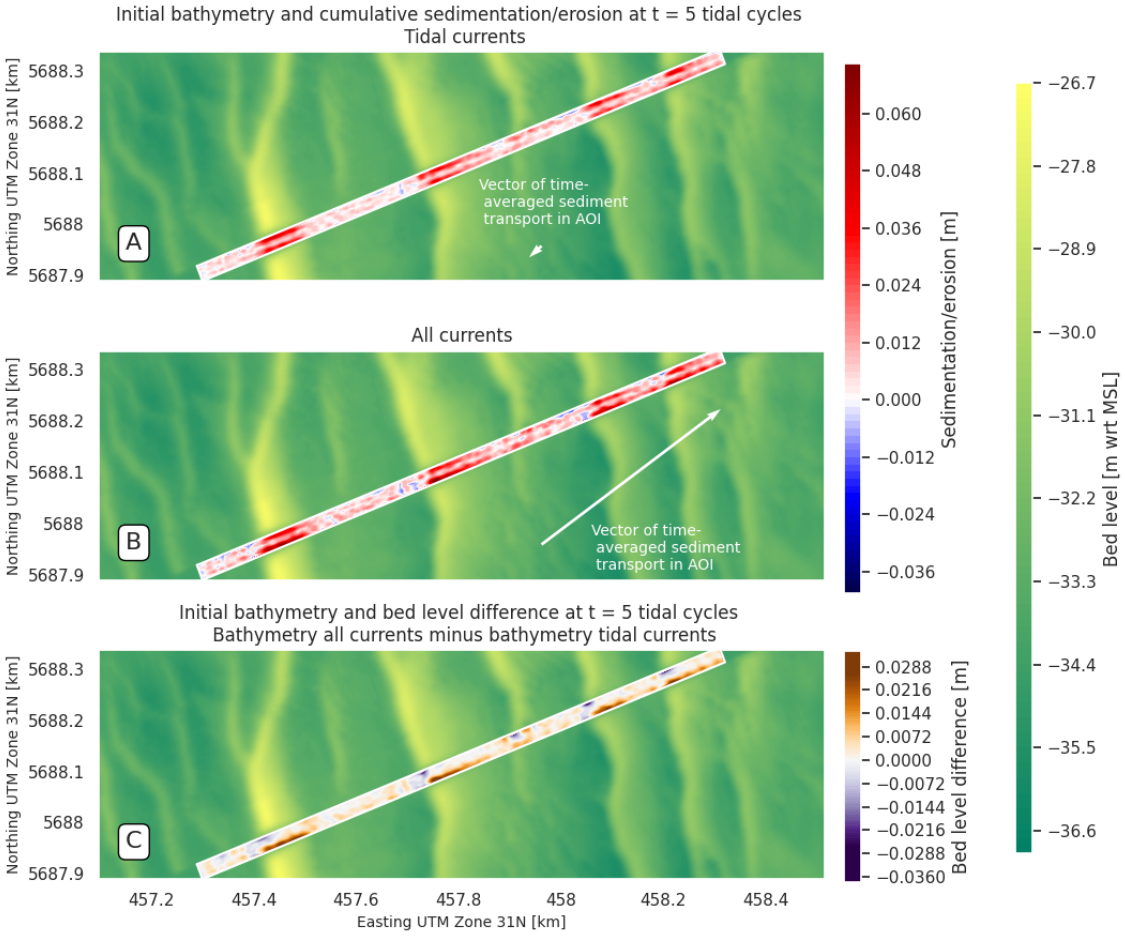

Figure 4.12: A,B: Cumulative sedimentation and erosion patterns after five tidal cycles focused on trench per simulation. C: Bed level difference after five tidal cycles in trench.

The sedimentation and erosion in the trench is also investigated in longitudinal direction. Again the bed level is retrieved at five transects, but now in the trench. The five transects are depicted in Figure figure 4.13. The results are shown in Figure 4.14. When comparing the sedimentation and erosion in both simulations, it can be observed that the near the crests of the sand waves the bed level increases more in the simulation which includes residual currents. A stronger erosion rate is also observed near the troughs of the sand waves. This is an indication that the residual currents contribute to an increase in the regeneration rate of the sand waves within the trench.

Last but not least, the changes in sediment budget within the trench are considered. These are depicted in Figure 4.15.

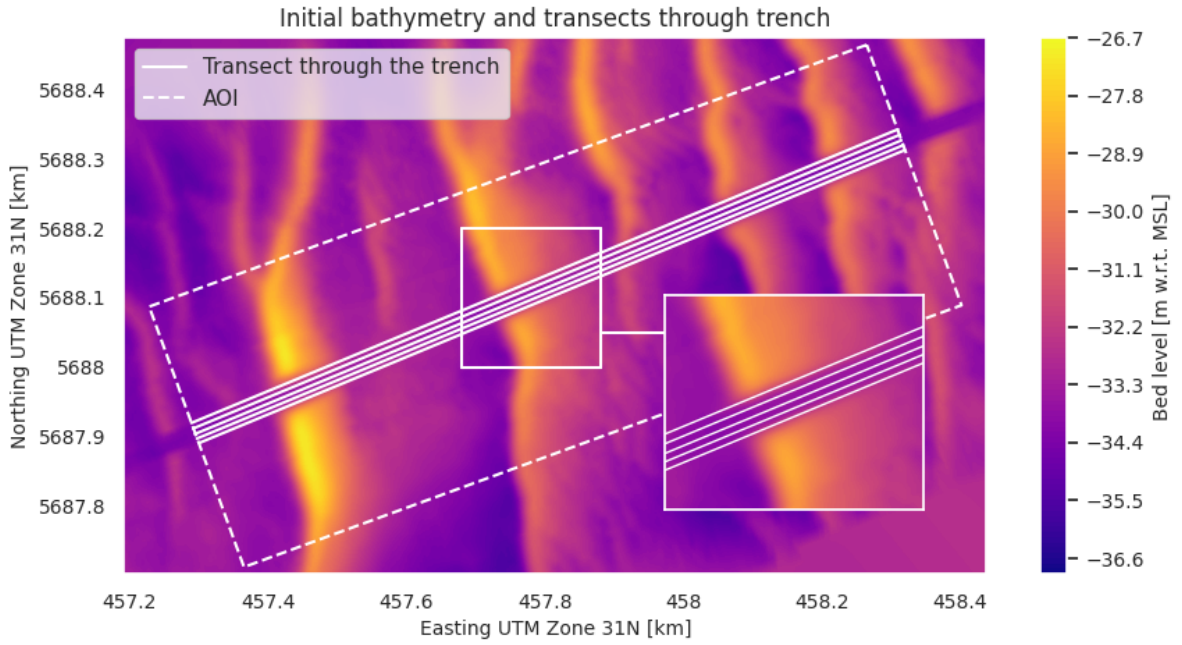

Figure 4.13: Transects in the trench.

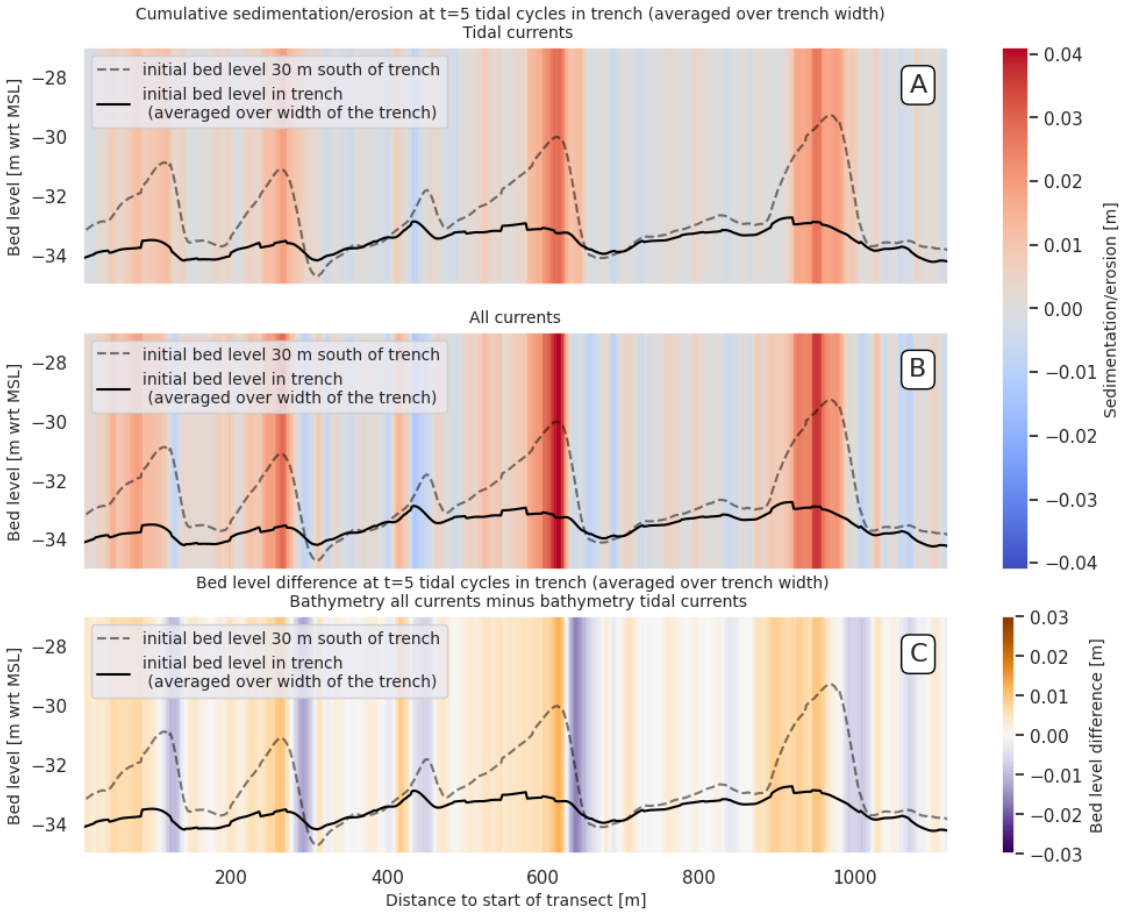

Figure 4.14: A,B: Sedimentation and erosion in transects through the trench. C: Bed level difference between two simulations in trench transects. The small peaks in the initial bed level in the trench can be attributed to the fact that the grid cells do not entirely align with the trench. Hence small peaks are observed on the locations where the grid cells switch.

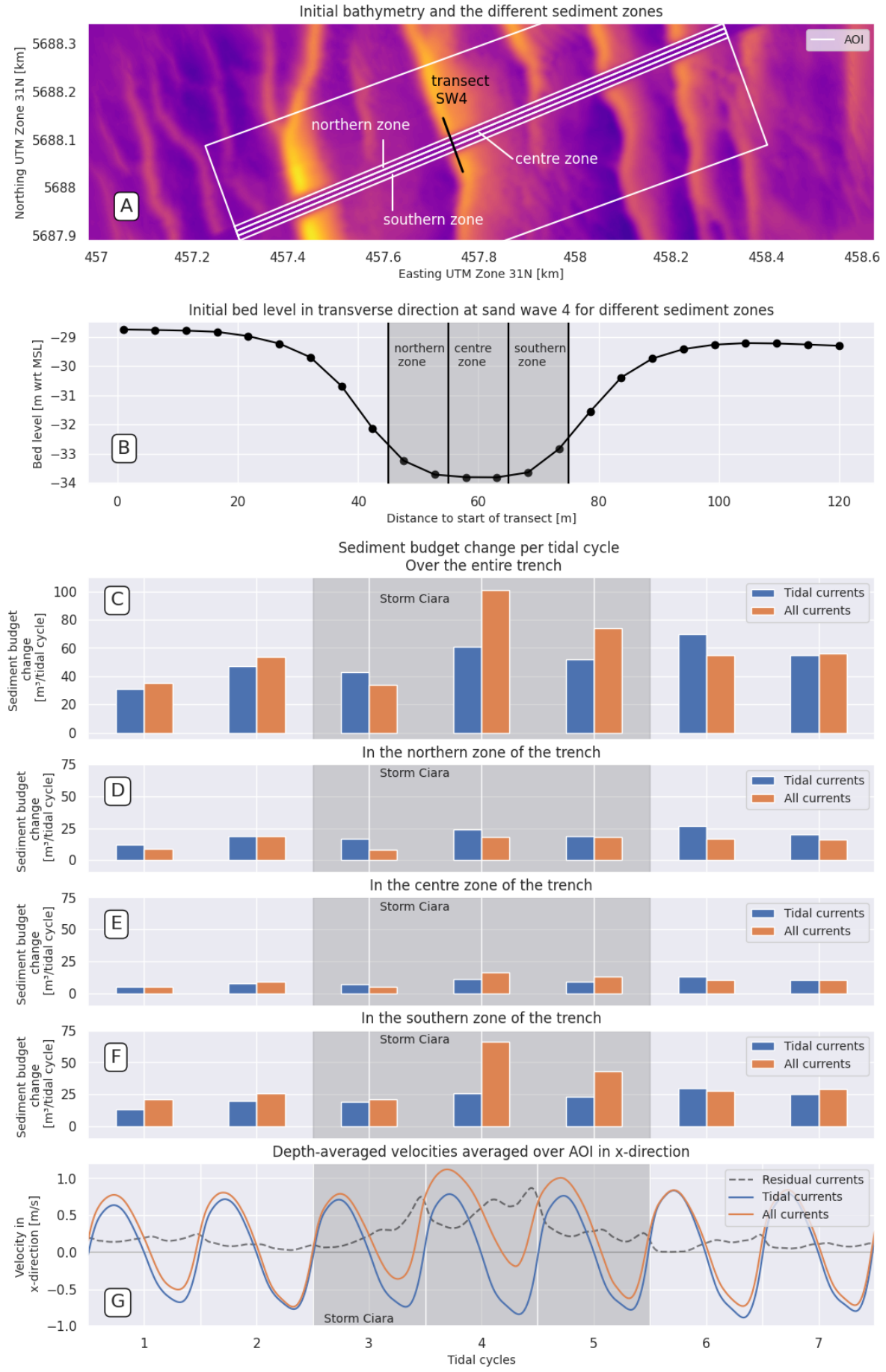

Figure 4.15: Sediment budget analysis in trench. A,B: indication different sediment zones. C,D,E,F: change in sediment budget per zone. G: Depth-averaged velocities per tidal cycle for reference.

A distinction is made between different zones within the trench. The different zones are depicted in subfigure A and a transect of the trench in transverse direction is shown in subfigure B. In subfigure C the sediment budget change is considered over the whole trench. During the third tidal cycle less sediment enters the trench in the simulation which includes all currents. In the next tidal cycle the opposite is true, here much more sediment infilling into the trench is observed. An increase of 66% to be exact. To explain this behaviour, the changes in sediment budget in the north and the south zone of the trench are analysed further. When looking at the northern zone, less sediment enters this zone of the trench during storm Ciara due to the residual currents. In the south, the opposite is true, here the residual currents increase the sediment budgets into the trench. Especially during the fourth tidal cycle this additional sediment infilling into the trench is significant. This can be explained by looking at the magnitudes of the residual currents which are depicted in subfigure G. The residual currents during the fourth tidal cycle are the highest, and they are directed in northeast direction. The majority of the sediment infilling into the trench is hence deposited in the trench on the lee side of the sand waves with respect to the incoming residual current. This is in line with the sedimentation and erosion patterns that were observed in the trench in Figure 4.12.

The previous analysis of the sediment budget within the trench is conducted for the sediment zones which do not include the slopes of the trench. In the next part the sediment budget change in the trench is analysed when the slopes are included and the area extends beyond the trench. Figure 4.16 shows the extended sediment zones and the associated trench transect in transverse direction.

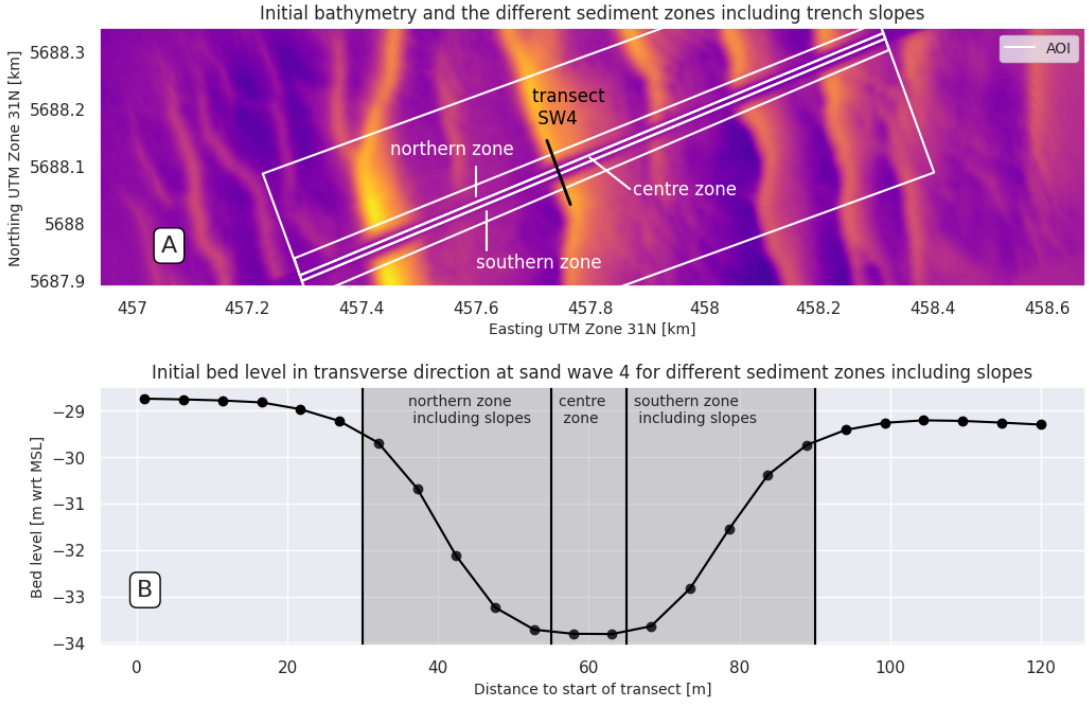

Figure 4.16: A: Different sediment zones including the slopes of the trench. B: Trench transect in transverse direction through sand wave 4 depicting the extend of the sediment zones including the slopes.

Figure 4.17 shows the total sediment budget change in the trench after five tidal cycles for the two types of sediment zones. After five tidal cycles, the sediment budget change in the total trench zone is 233 m^3 for the tide-only simulation which excludes the slopes, and 29 m^3 for the tide-only simulation which includes the slopes. This is an indication that a large part of the sediment entering the total trench zone (which excludes the slopes) originates from the slopes. Another interesting find is that the residual currents cause sediment infilling in the southern zone including the slopes, and ensure sediment leaves the northern zone when the slopes are included. This could be an indication the trench is migrating towards the north during storm Ciara.

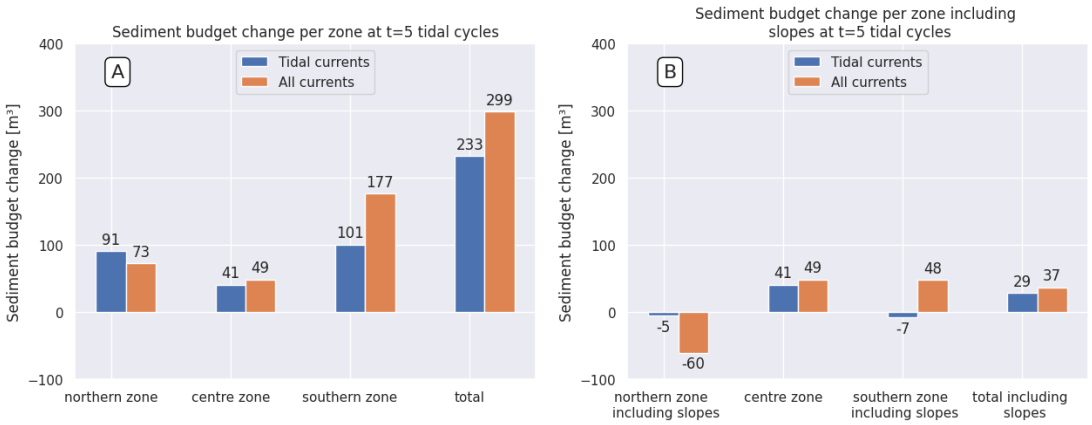

Figure 4.17: A: Total sediment budget change in trench during storm Ciara for sediment zones excluding trench slopes. B: The same, but now including the trench slopes.

4.4.3. Intermediate-term: Hydrodynamic differences

Figure 4.18A shows the depth-averaged velocity in x-direction averaged over the Area Of Interest for both simulations. Subfigure B and C depict the path of the depth-averaged currents during the 28 tidal cycles for both simulations.

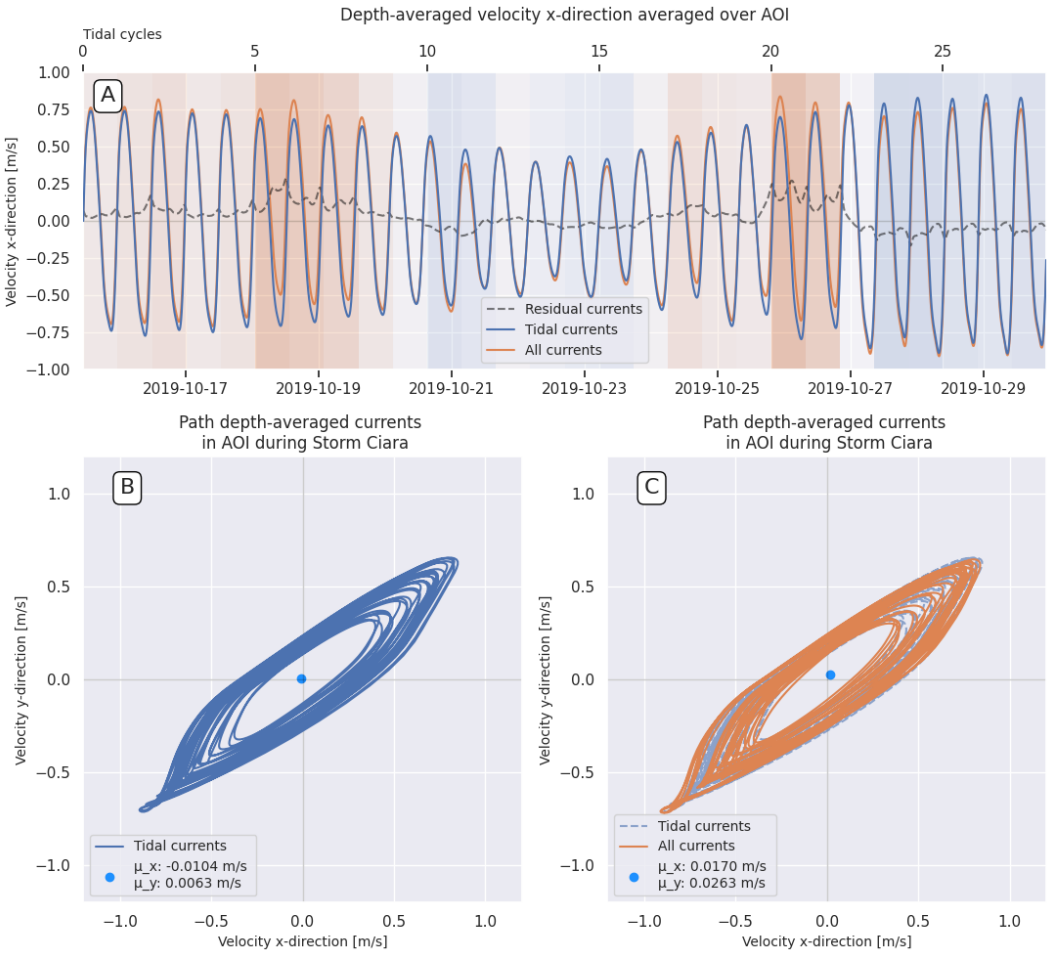

Figure 4.18: Hydrodynamic differences between the two model simulations. The orange background indicates that the residual currents averaged over one tidal cycle are positive and hence directed in northeast direction, the blue background indicates the same but for negative residual currents (southwest direction).

There are three moments in time when the residual currents, averaged over one tidal cycle, are relatively high. This is during the 19th of October and during the 26th of October, here the residual currents are directed towards the northeast. The other moment is during the last five tidal cycles (from the 27th and onwards), now the residual currents are directed towards the southwest. The currents averaged over space and time are very close to zero in both simulations, these currents are however slightly higher for the simulation which includes all currents, and are pointed towards the northeast.

4.4.4. Intermediate-term: Morphological differences

Both simulations show a similar sediment transport pattern as observed in the tide-only simulation of the short-term modelling scenario, except the magnitudes are higher now. There is erosion of the crests, and sedimentation at the troughs of the steep slopes of the sand waves. This is depicted in Figure 4.19A and B. Upon visual inspection it is difficult to see the differences in sedimentation and erosion patterns between the two simulations, hence Figure 4.20 depicts the bed level difference between the two simulations after 28 tidal cycles. In the simulation which only includes tidal currents, more sediment is deposited at the troughs of the steep slope and more sediment is eroded from the crests. This is an indication that the residual currents are reducing the migration rate of the sand waves. It must however be noted that the order of magnitudes of these differences is very small considering the sedimentation and erosion levels.

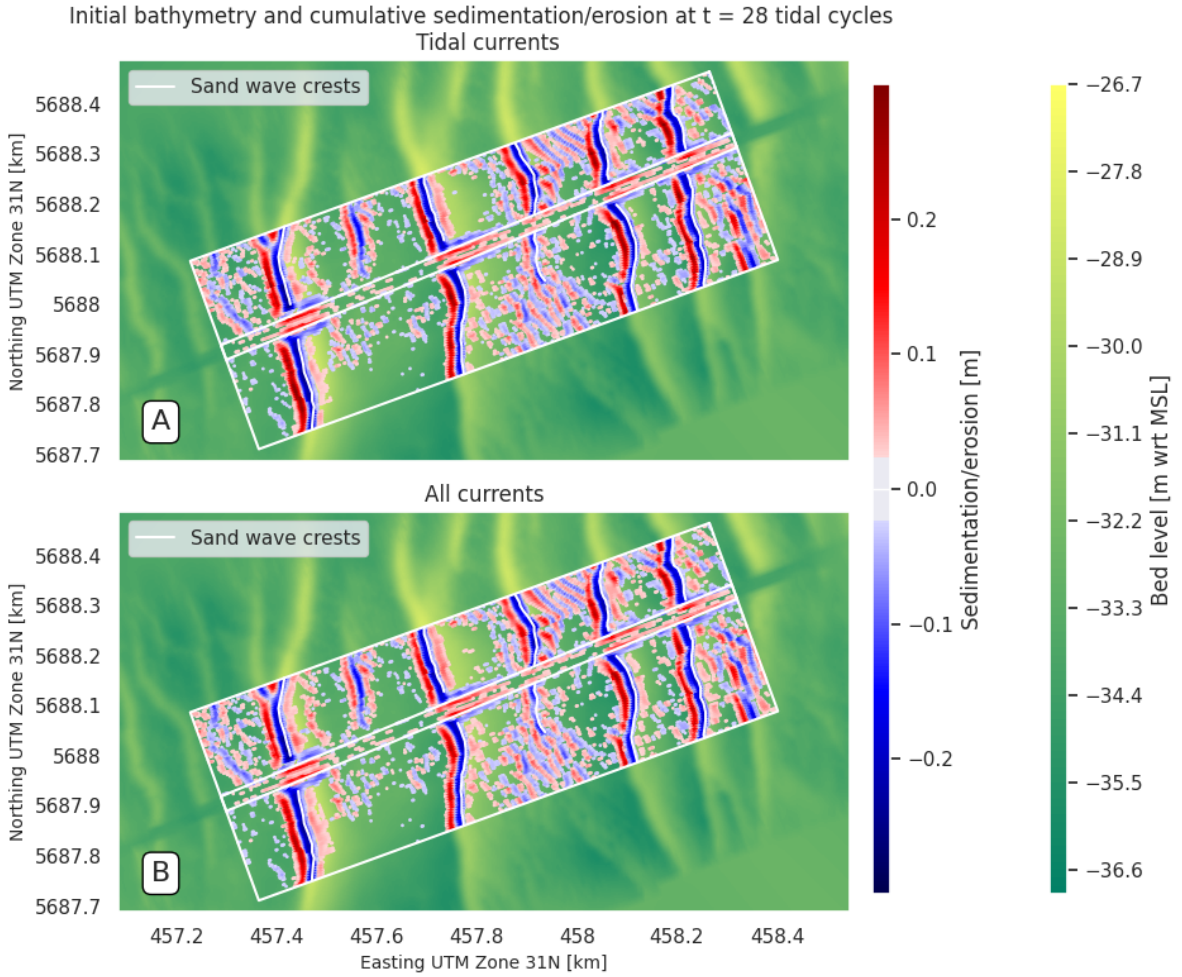

Figure 4.19: Cumulative sedimentation and erosion patterns after 28 tidal cycles

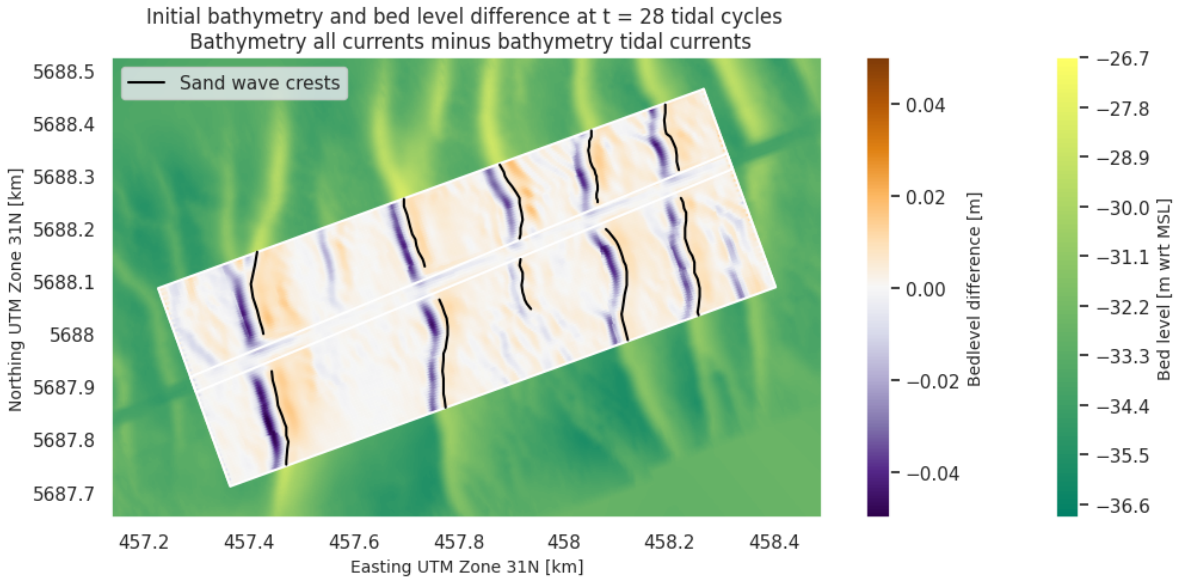

Figure 4.20: Bed level difference between the two simulations after 28 tidal cycles

In Figure 4.21 the sedimentation and erosion is shown again for the transect through the sand waves on the south of the trench. These emphasise that the sedimentation and erosion patterns in both simulations are the same, except the magnitudes are slightly higher for the simulation which includes only tidal currents.

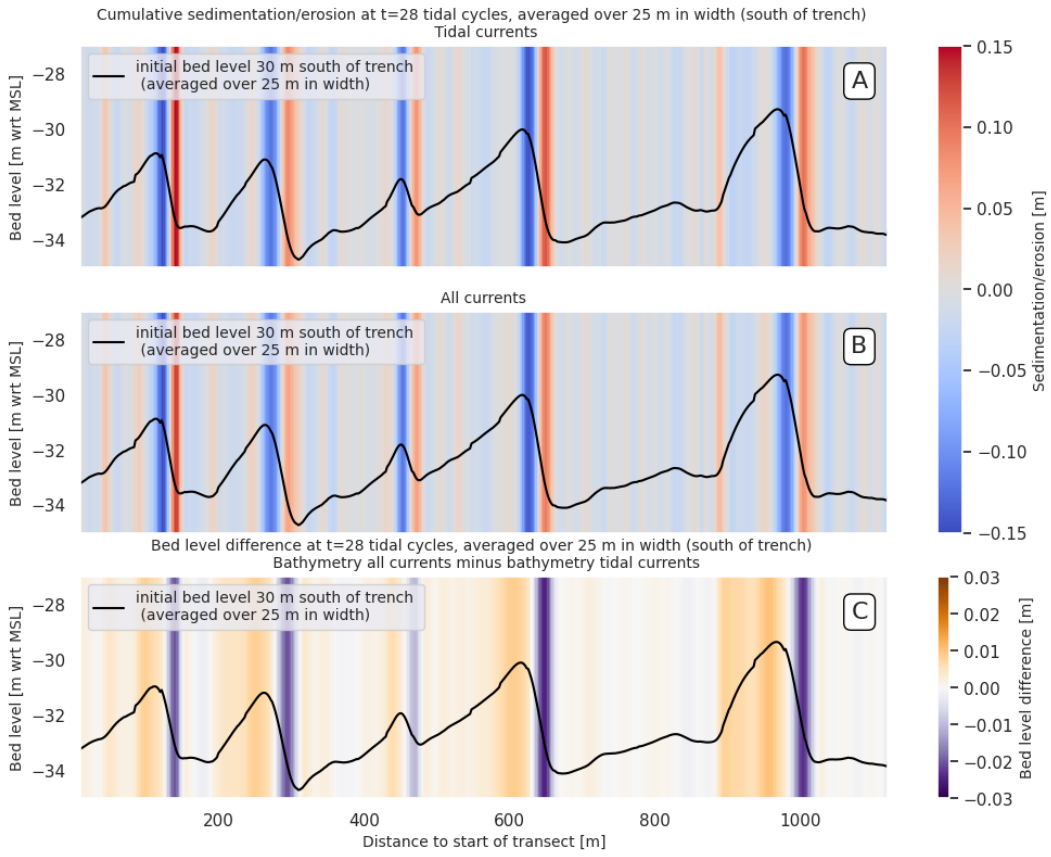

Figure 4.21: A,B: Sedimentation and erosion in transects through sand waves south of the trench. C: Bed level difference between two simulations in transects through sand waves south of the trench.

Morphodynamic behaviour within trench

Zooming in on the trench provides more insight into the effect of the residual currents on the interactions between the trench and the sand waves. Subfigure A and B of Figure 4.22 show the cumulative sedimentation and erosion after 28 tidal cycles in the trench. Again not much differences can be observed between the two simulations. In both simulations an even infilling in both sides of the trench is observed. When comparing the final bed levels between the two simulations, as is depicted in subfigure C, more sediment has entered the trench on the southern side in the simulation which includes residual currents, and less sediment has entered the trench on the northern side. However, the magnitudes of these differences are very small.

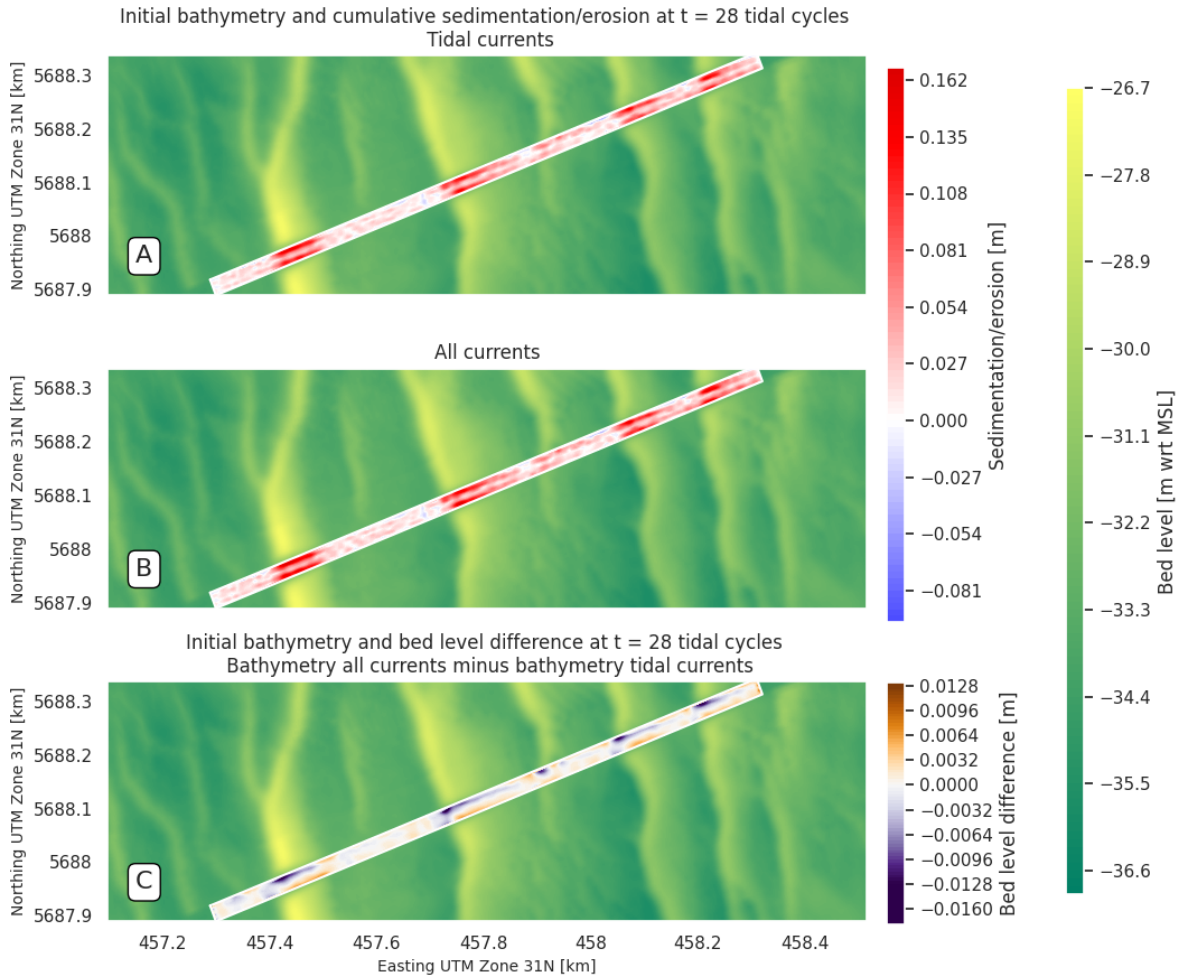

Figure 4.22: Cumulative sedimentation and erosion patterns and bed level difference after 28 tidal cycles focused on trench.

Finally, the sediment budgets inside the trench are investigated. Figure 4.23 shows the sediment budget changes after 28 tidal cycles per zone. Again, two types of sediment zones are considered. One which does not include the slopes (Subfigure A and B of Figure 4.15) and one which does include the slopes (Figure 4.16). It becomes obvious that after 28 tidal cycles, there is hardly any difference between the two simulations in terms of sediment budget for both different types of sediment zones. Within the trench (excluding the slopes), a decrease of 3% in sediment infilling is observed due to the residual currents. This can be explained by the fact that there is a larger decrease in sediment infilling on the northern side of the trench compared to the increase on the southern side. However these differences are small, hence 3% decrease is not significant and can also be subject to the definition of the three zones. When considering the zones which include the slopes, again there is hardly any change in sediment budget in the northern and southern part, adding to the belief that the sediment is eroded from the higher part of the slopes and deposited on the troughs.

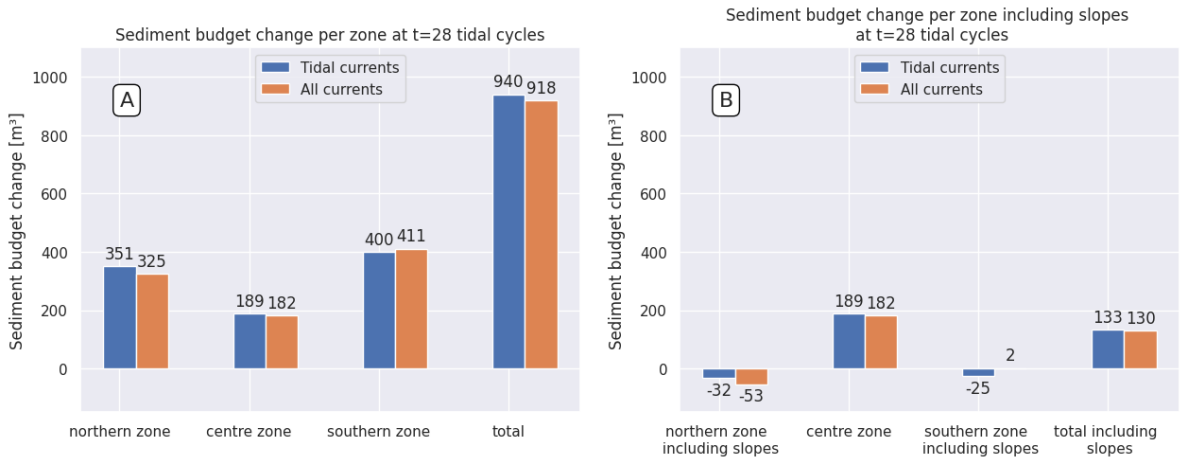

Figure 4.23: A: Sediment budget change in trench excluding the trench slopes. B: The same but now including the slopes.

When looking at the sediment budget changes per tidal cycle inside the trench in Figure 4.24 there are however relatively bigger differences to be observed between the two simulations. When the residual currents are higher and directed towards the northeast, there is less infilling into the north of the trench and there is more infilling into the south of the trench. When the residual currents are pointed towards the southwest, the effect is opposite. When the residual currents are higher the effects on the sediment infilling are higher. It is also important to pay attention to the amounts of infilling during neap tide and during spring tide. During neap tide, the depth-averaged velocities are still in the order of magnitudes of about 0.5 m/s, however there is hardly any infilling into the trench. During spring tide the depth-averaged velocities are higher (roughly 0.8 m/s), and there is much more sediment entering the trench. Compared to the effects of the residual currents, the contributions of the spring-neap tidal cycle are much higher.

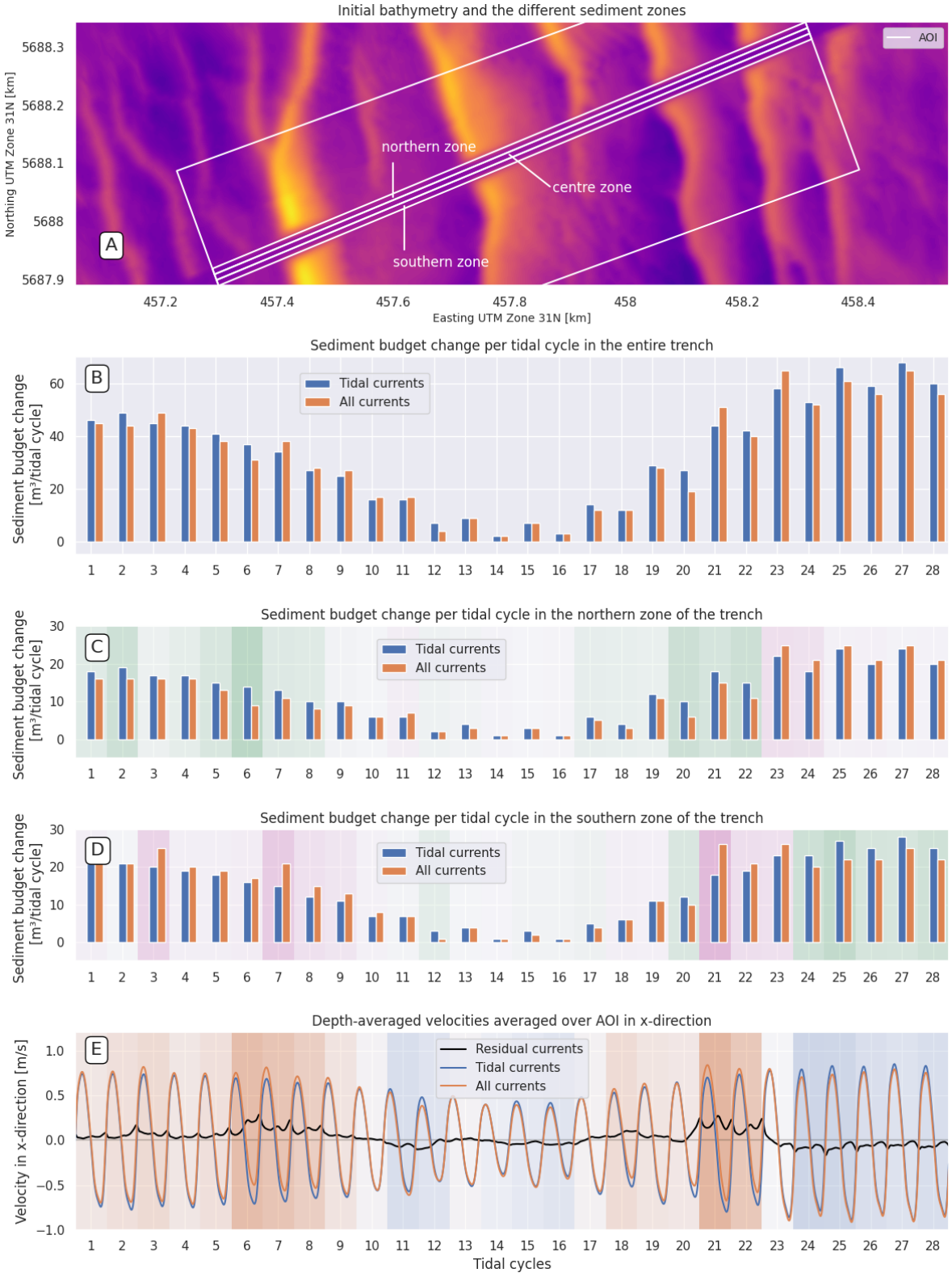

Figure 4.24: A: Different sediment zones. B,C,D: Sediment budget change over the entire trench, in the northern zone, and in the southern zone respectively. A green background indicates there is more infilling in the tide-only simulation, and a pink background indicates there is more infilling in the simulation which includes all currents. E: Depth-averaged velocities in x-direction, averaged over the Area Of Interest.

5
Discussion

In this chapter, the most important implications and assumptions of the results presented in the previous chapters are discussed. First, the interactions between the residual currents and the variations in spring-neap tide are elaborated. This is followed by a consideration of the case study from a broader perspective. Finally, missing physical mechanisms and parameters in the numerical model and their implications are commented on.

5.1. Timing with respect to the tide

The ratio between sediment infilling into the trench caused by residual currents and those caused by tidal currents strongly depends on the timing of the residual currents with respect to the variations in the spring-neap tide. In section 4.4.4 it was found that during neap tide there was hardly any sediment infilling into the trench, whereas during spring tide the sediment infilling was several orders of magnitude higher (see Figure 4.24). Hence for this case study, the threshold value for sediment mobility lies somewhere near the peak tidal velocities during neap tide. During the peak of storm Ciara, a 66% increase in sediment infilling into the trench was observed compared to tide-only conditions. Storm Ciara occurred just before the peak in spring tide. If storm Ciara had occurred during neap tide, the residual currents would have caused a relatively larger increase in velocity. The threshold value would have surely been exceeded and a relatively larger amount of sediment infilling would have occurred with respect to the infilling by the tide only. This would eventually result in a relatively larger sediment infilling caused by the residual currents, compared to when storm Ciara occurs during spring tide. It is not expected that the ratio will change substantially, but it should be kept in mind that the exact numerical value of the ratio is subject to the timing of the residual currents with respect to the spring-neap tide variations.

5.2. Case study in broader perspective

Case study characteristics

The case study concerns a dredged trench within a group of sand waves in the Belgium Continental Shelf. The case study is unique given a set of characteristics which are expected to influence the system in their own way. The characteristics with the largest implications are discussed here. As mentioned before the variations in spring-neap tide play a large role in the sediment infilling into the trench. These variations are in turn dependent on the relative amplitudes of the M2 (lunar) and S2 (solar) constituents. When these are in the same order of magnitude, a large difference in amplitude is observed between spring and neap tide. Hence, exerting a relatively larger influence on the sediment infilling than when the amplitudes are not in the same order of magnitude. Threshold velocities can also play a large role, in the previous section it was already explained that during neap tide the velocities are close to the threshold of sediment mobility. The closer the tidal velocities are to this threshold, the larger the relative influence of the residual currents can be. Trench configuration with respect to the sand wave crests, tidal axes, and residual current directions are hypothesised to influence the way sediment is distributed in the system. In this case study, the trench is aligned (almost) parallel to the directions of flood and ebb tide and to the dominant directions of the highest residual currents (southwest and northeast). It is hypothesised that if the trench had a more perpendicular configuration with respect to the tidal

axes and residual current directions more infilling of sediment into the trench would be expected, as the flow velocities are then pointed towards the trench instead of parallel to it. Sand wave systems are by definition tidally dominated, it is therefore expected that residual currents will have limited influence on the morphodynamics in other case studies as these are also tidally dominated. However, the effects the previously mentioned characteristics (and other characteristics which are not mentioned here) can have on the morphodynamics should be kept in mind when evaluating a sand wave and trench system to be able to confidently exclude residual currents.

Storm Ciara in perspective

Storm Ciara induced residual currents which are amongst the highest residual currents observed over a three year period in the Area Of Interest. It is unknown how the residual currents induced by storm Ciara exactly relate to the residual currents caused by other storm events in the past, but it is known that storm Ciara is mentioned in the list of heavy storms that have occurred in the Netherlands since 1910 (KNMI, n.d.). During storm Ciara an increase of 0.4 m/s in currents in northeast direction was observed during peak tidal velocities. This caused a tripling of the sediment transport in that direction, as depicted in 4.7. Nevertheless, only an increase of 66% of sediment infilling into the trench was observed due to the residual currents. This can be attributed to the fact that the residual currents increased sediment infilling into the south of the trench, but they also decreased sediment infilling into the north of the trench. Comparing this infilling rate to the infilling rate due to the tide only, this amount of infilling is already made up for by one tidal cycle. Hence, this amount of infilling due to the residual currents during storm Ciara is negligible over increased periods of time.

5.3. Influence of missing physical mechanisms and parameters

Sand wave dampening

Although in general the sand wave behaviour seems to be captured well in the numerical model, a dampening of the sand waves is observed. This phenomenon is especially visible in the sedimentation and erosion plots during the tide-only simulations (Figure 4.8 & 4.19). Theory dictates that flow is contracted on the crest of the sand waves and hence accelerates. After the crest of the sand waves, the flow decelerates again. Erosion is expected on the crest, and deposition is expected to occur in the direction of migration of the sand wave. In the NEMO model, erosion occurs on the crest, however this erosion extends up to about halfway onto the steep slope. As deposition is expected to occur at these locations a dampening of the sand waves is implied. The extent of this dampening is however limited, and does not dominate the behaviour of the sand waves. For example, in the simulation which includes residual currents, erosion occurs on the steep slopes instead of deposition. The dampening of the sand waves was also present in the model from the thesis of Tam (2023). It was hypothesised that it could be attributed to numerical causes, for instance the artificial diffusion caused by the numerical schemes of sediment transport, or that the reason may be due to any missing physical mechanisms that simulate up-slope transport. Unfortunately, the residual currents simulated in this thesis do not function as that missing mechanism. Another potential measure to counteract the sand wave dampening are tuning the bed slope parameters. In this thesis the default values are used for the transverse and longitudinal bed slope parameter. A larger bed slope parameter increases down-slope sediment transport in that direction. The bed slope parameters, in combination with the sediment transport formulation, can strongly influence the growth rate of sand waves (Choy, 2015). Tuning these parameters could limit down-slope transport and counteract the dampening of the sand waves. In view of time it was not possible to calibrate the parameters, but it is recommended to do so in the future.

Comparison to measurements

Comparing the results of the sediment budget analysis of the representative period (Figure 4.23) to the sediment budget analysis of the measurements (Figure 3.5) provides additional insights in model skill compared to the real-life measurements. To begin with, the measurements show a larger increase in sediment budget in the centre zone of the trench relative to the other zones, whereas the NEMO model shows a relatively lower increase in sediment budget in the centre zone compared to the other zones. This mismatch in sediment budget ratio can be attributed to a number of reasons. Firstly, two different time frames are considered. The measurements cover the infilling over a period of three years, whereas the model considers sediment infilling over two weeks. It is likely that at first the sediment is

deposited in the trench near the slopes, and then slowly starts to fill up the trench up until the other two sides reach each other. Another reason could be the exclusion of suspended load transport in the model, which can influence the locations of sediment infilling into the trench. Suspended load transport accounts for sediment grains which are brought into suspension. Suspended sediment does not react instantaneously to currents which allows sediment to be deposited more evenly and further away from the slopes of the trench, leading to additional infilling in the centre of the trench.

In both the measurements and the model the southern side of the trench seems to have a larger increase in sediment budget than the northern side, the exact ratios can be found in Table 5.1.

Type of sediment budget analysis	Sediment infilling in southern zone	Sediment infilling in northern zone	Ratio
Measurements	85307 m^3	68144 m^3	1.25
NEMO intermediate term - tidal currents	400 m^3	351 m^3	1.14
NEMO intermediate term - all currents	411 m^3	325 m^3	1.26

Table 5.1: Ratio between sediment infilling in southern zone versus northern zone. Derived from Figure 3.5 and Figure 4.23.

As the ratio is 1.14 for the simulation which only includes tidal forcing, a portion of the dominance of sediment budget infilling into the south of the trench can be attributed to the (asymmetries in) tidal forcing. The remainder can be attributed to the residual currents, which hinder sediment infilling in the northern zone and increase sedimentation rates in the southern zone, which results in a ratio of 1.26. Comparing this to the ratio of infilling of the measurements which is 1.25, adds to the belief that the residual currents contribute to improving the way sediment is distributed over the trench compared to tide-only conditions. Still it should be kept in mind that two different time periods are considered here.

Influence of waves

The influence of waves on morphodynamics is not considered in this thesis. To make a simple quantitative approximation of the influence waves could have, the bed shear stresses due to two different wave conditions are calculated and compared to the bed shear stresses caused by the currents in this thesis. Bed shear stress is an indicator of sediment mobility, and is non-linearly related to sediment transport ($S \sim \tau^{1.5}$). Appendix A refers to the detailed calculation and assumptions. It was found that the bed shear stresses caused by waves during a storm could be significant, whereas the bed shear stresses caused by waves during representative conditions were negligible. The bed shear stress caused by waves during storm conditions ($H_s = 5.2\ m$) can be twice as large as the bed shear stress caused by the tidal currents and residual currents during a storm. Campmans (2018) explains that waves enhance sand wave migration which is caused by other processes; waves stir up sediment from the bed by their orbital motions, and the sediment is then transported by the currents and deposited elsewhere. The waves during storm conditions are thus expected to increase the bed shear stresses and consequently the sediment transport magnitudes, but are not expected to alter the sediment transport patterns. The bed shear stresses caused by the waves under representative conditions ($H_s = 1.2\ m$) were several orders of magnitude smaller than the bed shear stress caused by the tide only, and are hence considered insignificant.

6

Conclusions and Recommendations

6.1. Conclusions

The aim of this thesis is to investigate the effects residual currents can have on the interactions between sand waves and trenches, such that ultimately these systems can be understood better and more adequate and efficient designs and maintenance procedures of offshore wind systems can be proposed. The main research question of the thesis is as follows: “How do residual currents influence the morphological interactions between sand waves and trenches?”. Before answering the main research question, the answers to the subquestions are provided first.

1. “What are the characteristics of residual currents in the Area Of Interest over the period of 2018-2021, and which forcing mechanisms induce these currents?”

The residual currents observed in the Area Of Interest over the period of 2018-2021 are directed along two main axes: the northeast and the southwest. The orientations of these axes coincide with the direction of flood and ebb flow respectively. Considering the occurrence probability and the magnitudes of the mean and maxima in each direction, a distinct dominance towards the northeast axis (flood direction) is observed. The highest residual currents over the three year period reach 1 m/s, but the majority of the time (85%) the magnitudes of the residual currents are below 0.15 m/s. Wind and atmospheric pressure are the main drivers behind the generation of the residual currents in this area.

2. “How do event-driven residual currents influence the interaction between sand waves and trenches?”

A numerical model is used to study the influence of residual currents on a trench within a group of sand waves during a storm. During the tidal cycle in which the residual currents reached their peak, a 66% increase in sediment infilling into the trench was observed compared to tide-only conditions. Considering two tidal cycles occur per day, this additional infilling is negligible compared to the effects of the tide over an increased period of time. Despite the limited influence of the residual currents in terms of sediment budget, the residual currents are strong enough to be able to reverse the bed load transport patterns. Sediment is eroded from the steep slopes of the sand waves and deposited on the gentle slopes, which opposes the behaviour observed during tide-only conditions. Additionally, more sediment infilling was observed in the southern part of the trench, which coincides with the part of the trench that is on the lee side of the sand waves compared to the incoming current. On top of this, the residual currents were also found to contribute to an increase in regeneration rate of the sand waves inside the trench.

3. “How do residual currents influence the interactions between sand waves and trenches during representative hydrodynamic conditions?”

The same numerical model is used, but now the influence of representative residual currents is studied over a fourteen day period (one spring-neap tidal cycle). It was found that the residual currents mostly influence the location of sediment infilling into the trench. The magnitudes of these effects are however small, especially compared to the influence of the spring-neap tide which seems to play a much larger role. When the residual currents are directed towards the northeast, more sediment infilling is observed in the southern part of the trench and less sediment enters the trench on the northern side. When the

residual currents are directed in opposite direction, this effect is reversed. As the direction of the residual currents varied over time, the effects on the sediment infilling into the trench roughly cancelled each other after one spring-neap tidal cycle. It was also found that the residual currents ensured less sedimentation on the troughs of the steep slopes of the sand waves and less erosion on the crests and the gentle slopes, indicating a decrease in migration rate of the sand waves.

"What role do residual currents play in the morphological interaction between sand waves and trenches?"

The residual currents observed in this case study are able to influence the location of sediment infilling into the trench and can increase the regeneration rates of sand waves within the trench due to increased sediment transport rates. The magnitudes associated with these morphological changes are however considered small. Especially when relating these changes to the influence of spring-neap tide variations on the morphodynamics, which is several orders of magnitude larger. It is therefore concluded that residual currents play no significant role in the morphological interaction between sand waves and trenches for this case study.

6.2. Recommendations

From this case study, it becomes clear that the influence of the spring-neap tide outweighs the influence of the residual currents. Spring tide occurs when the M2 and S2 components are in phase, and neap tide occurs when they are out of phase. It is hence crucial that in further research both M2 and S2 components are included to be able to simulate the effects of the spring-neap tidal cycle. It is hypothesised that residual currents in other case studies are not likely to induce large morphological changes, as those systems will also likely be tidally dominated. Therefore, when the interest lies in examining the morphological evolution of sand waves and trenches over increased periods of time, it is expected that the inclusion of one spring-neap tidal cycle in combination with a morphological scaling parameter will be sufficient. For further research it is additionally recommended to investigate the influence of the bed slope parameters on the dampening observed of the sand waves in the Delft3D FM model.

For practical applications of this research it is recommended to make use of the observed influences of the variations of the spring-neap tide on the morphodynamics. For instance, it wise to dredge a trench during neap tide as the least morphological change is expected to occur in this period. Additionally it was discovered in this research that more sediment infilling occurred in the southern zone of the trench with respect to the northern zone. This can be partly attributed to the asymmetry in the tide, and partly attributed to the residual currents which can influence the location of sediment infilling into the trench. Knowing which side of the trench will regenerate sooner may be useful for engineering purposes. It is also advised to contemplate the configuration of the trench with respect to the tidal axes and dominant directions of the residual currents. It is expected that if these flows are parallel to the trench, the sediment infill rates into the trench will likely be lower.

References

Amos, C., & King, E. (1984). Bedforms of the canadian eastern seaboard: A comparison with global occurrences. *Marine Geology*, *57*, 167–208. https://doi.org/10.1016/0025-3227(84)90199-3

Auguste, C., Marsh, P., Nader, J., Penesis, I., & Cossu, R. (2021). Modelling morphological changes and migration of large sand waves in a very energetic tidal environment: Banks strait, australia. *Energies*, *14*, 3943. https://doi.org/10.3390/en14133943

Bao, J., Cai, F., Shi, F., Wu, C., Zheng, Y., Lu, H., & Sun, L. (2020). Morphodynamic response of sand waves in the taiwan shoal to a passing tropical storm. *Marine Geology*, *426*. https://doi.org/10.1016/j.margeo.2020.106196

Bao, J., Cai, F., Wu, C., Lu, H., Zheng, Y., Li, Y., Sun, L., Liu, C., & Li, Y. (2023). Regeneration and anti-migration of sand waves associated with sand mining in the taiwan shoal. *Acta Oceanologica Sinica*, *42*, 71–78. https://link.springer.com/article/10.1007/s13131-023-2162-1

Besio, G., Blondeaux, P., Brocchini, M., & Vittori, G. (2003). Migrating sand waves. *Ocean Dynamics*, *53*, 232–238. https://doi.org/10.1007/s10236-003-0043-x

Bokuniewicz, H., Gordon, R., & Kastens, K. (1977). Form and migration of sand waves in a large estuary, long island sound. *Marine Geology*, *24*, 185–199. https://doi.org/10.1016/0025-3227(77)90027-5

Borsje, B., Kranenburg, W., Roos, P., Matthieu, J., & Hulscher, S. (2014). The role of suspended load transport in the occurrence of tidal sand waves. *Journal of geophysical research: Earth surface*, *119*(4), 701–716. https://doi.org/10.1002/2013JF002828

Borsje, B., Roos, P., Kranenburg, W., & Hulscher, S. (2013). Modeling tidal sand wave formation in a numerical shallow water model: The role of turbulence formulation. *Elsevier: Continental Shelf Research*, *60*. https://www.utwente.nl/en/et/cem/research/wem/people-attachments/borsje/borsje-etal-2013-csr.pdf

Bosboom, J., & Stive, M. (2023). *Coastal dynamics*. TU Delft Open. https://textbooks.open.tudelft.nl/textbooks/catalog/view/37/92/383

Caires, S., Tzampazidou, E., & Saleh, M. (2024). Princess elisabeth zone measurement campaign validation of the post-processed campaign data (nov. 2022 - nov. 2023).

Campmans, G. (2018, August). *Modeling storm effects on sand wave dynamics* [PhD Thesis - Research UT, graduation UT]. University of Twente. University of Twente. https://doi.org/10.3990/1.9789036546003

Campmans, G., Roos, P., van der Sleen, N., & Hulscher, S. (2021). Modeling tidal sand wave recovery after dredging:effect of different types of dredging strategies. *Coastal Engineering*. https://ris.utwente.nl/ws/portalfiles/portal/250822961/10.1016_j.coastaleng.2021.103862.pdf

Choy, D. (2015). Numerical modelling of the growth of offshore sand waves. https://repository.tudelft.nl/islandora/object/uuid%3A35e168b6-4d39-4e12-becd-4bbd701372d0

Council, G. W. E. (2020). *Oreac: 1,400 gw of offshore wind is possible by 2050, and will be key for green recovery*. Retrieved June 8, 2020, from https://gwec.net/oreac-1400-gw-of-offshore-wind-is-possible-by-2050-and-will-be-key-for-green-recovery/

Damen, J., van Dijk, T., & Hulscher, S. (2018). Spatially varying environmental properties controlling observed sand wave morphology. *Journal of Geophysical Research: Earth Surface*, *123*, 209–408. https://doi.org/10.1002/2017JF004322

Deltares. (2018). *The 3d dutch continental shelf model - flexible mesh (3d dcsm-fm) - setup and validation*. https://www.deltares.nl/en/expertise/publicaties/3d-dutch-continental-shelf-model-flexible-mesh-3d-dcsmfm-setup-and-validation

Deltares. (2023a). *Delft3d fm suite 2d3d*. https://www.deltares.nl/en/software-and-data/products/delft3d-flexible-mesh-suite

Deltares. (2023b). *Impact report: Upscaling offshore wind energy*. https://specials.deltares.nl/impact_report_2023/upscaling_offshore_wind_energy

Deltares. (2024). *Delft3d fm user manuals*. https://oss.deltares.nl/web/delft3dfm/manuals

EMODnet. (2021). *Emodnet bathymetry - which information layers?* [accessed 18-05-2023]. https://www.emodnet-bathymetry.eu/data-products/which-information-layers

Hulscher, S. (1996). Tidal induced large scale regular bed form patterns in a three dimensional shallow water model. *Journal of geophysical research: Oceans*.

Hulscher, S., & van den Brink, G. M. (2001). Comparison between predicted and observed sand waves and sand banks in the north sea. *Journal Of Geophysical Research: Oceans*, *106*(C5), 8957–9638. https://doi.org/10.1029/2001JC900003

Jonsson, I. (1967). Wave boundary layers and friction factors. *Proceedings of the 10th Internation Conference on Coastal Engineering*, *2*, 127–148.

KMI. (2020). *Storm ciara*. https://www.meteo.be/nl/info/nieuwsoverzicht/storm-ciara

Knaapen, M. (2005). Sandwave migration predictor based on shape information. *Journal of Geophysical Research: Earth Surface*, *110*. https://doi.org/10.1029/2004JF000195

KNMI. (n.d.). *Zware stormen in nederland sinds 1910*. https://www.knmi.nl/nederland-nu/klimatologie/lijsten/zwarestormen

Krabbendam, J., Roche, M., Lancker, V. V., Nnafie, A., Terseleer, N., Degrendele, K., & Swart, H. D. (2022). Do tidal sand waves always regenerate after dredging? *Marine Geology*, *451*. https://doi.org/10.1016/j.margeo.2022.106866

Larsen, S., Roulund, A., & MCIntyre, D. (2020). Regeneration of partially dredged sandwaves.

Leenders, S. (2018). Numerical modelling of the migration direction of offshore sand waves using delft3d. https://repository.tudelft.nl/islandora/object/uuid%3Aae051d49-e639-460f-ba92-7305857ba592

Link, N. (2013). *Environmental statement volume i*. https://www.yumpu.com/en/document/view/50497655/nemo-link-uk-marine-environmental-statement

Luijendijk, A. P., de Schipper, M. A., & Ranasinghe, R. (2019). Morphodynamic acceleration techniques for multi-timescale predictions of complex sandy interventions. *Journal of Marine Science and Engineering*, *7*(3). https://doi.org/10.3390/jmse7030078

Morelissen, R., Hulscher, S. J., Knaapen, M. A., Németh, A. A., & Bijker, R. (2003). Mathematical modelling of sand wave migration and the interaction with pipelines. *Coastal Engineering*, *48*(3), 197–209. https://doi.org/https://doi.org/10.1016/S0378-3839(03)00028-0

National Grid (UK) and Elia (BE). (2018). *NEMO LINK - bathymetry surveys*.

Ørsted. (2018). *Appendix 11 to deadline i submission – sandwave clearance clarification note*. Retrieved November 7, 2018, from https://infrastructure.planninginspectorate.gov.uk/wp-content/ipc/uploads/projects/EN010080/EN010080-001133-DI_HOW03_Appendix%2011.pdf

Overes, P. (2021). Modeling sand wave field dynamics in the north sea using delft3d flexible mesh. https://repository.tudelft.nl/islandora/object/uuid%3A492ee814-9821-4943-aa16-6299fcf7533e

Overes, P., Borsje, B., Luijendijk, A., & Hulscher, S. (2024). The importance of time-varying, non-tidal currents in modelling in-situ sand wave dynamics. *Coastal Engineering*, 104480. https://doi.org/https://doi.org/10.1016/j.coastaleng.2024.104480

Ranasinghe, R., Swinkels, C., Luijendijk, A., Bosboom, J., Roelvink, D., Stive, M., & Walstra, D. (2011). Morphodynamic upscaling with the morfac approach. *Coastal Engineering Proceedings*, *32*. https://doi.org/10.9753/icce.v32.sediment.59

Rijksoverheid. (2023). *Windparken op zee: Nederland ruim op schema, begin 2024 start tenderronde voor verdubbeling*. Retrieved December 20, 2023, from https://www.rijksoverheid.nl/onderwerpen/duurzame-energie/nieuws/2023/12/20/windparken-op-zee-nederland-ruim-op-schema-begin-2024-start-tenderronde-voor-verdubbeling

Sterlini, F., Hulscher, S., & Hanes, D. (2009). Simulating and understanding sand wave variation: A case study of the golden gate sand waves. *Journal of Geophysical Research: Earth Surface*, *114*. https://doi.org/10.1029/2008JF000999

Swart, D. (1974). Offshore sediment transport and equilibrium beach profiles. *(Doctoral dissertation)*.

Tam, Z. (2023). Simulating 3d sand wave recovery after pre-sweeping by delft3d fm. https://repository.tudelft.nl/islandora/object/uuid%3Ad6b8ad7d-d362-4b5c-b96a-ebd121b58104

Tonnon, P., van Rijn, L., & Walstra, D. (2006). The morphodynamic modelling of tidal sand waves on the shoreface. https://www.leovanrijn-sediment.com/papers/P7-2007b.pdf

Vindenes, H., Orvik, K., Søiland, H., & Wehde, H. (2018). Analysis of tidal currents in the north sea from shipboard acoustic dopplercurrent profiler data. *Continental Shelf Research*, *162*. https://doi.org/10.1016/j.csr.2018.04.001

A

Wave influence on bed shear stress

Due to the relatively large depth of the seabed of the Area Of Interest and due to software limitations, it was decided not to include the effects of waves in this thesis. Waves can influence the results of this thesis in two ways. Firstly, waves can be responsible for the generation of residual currents, just like wind, atmospheric pressure, and density differences. Including waves could therefore have influenced the outcome of the analysis performed on the residual currents with the DCSM. Another way in which waves could have influenced the outcomes presented in this thesis, is in the way they influence the hydrodynamics. Waves are known to introduce oscillatory motions into the water column. These orbital motions, when reaching a critical value, are likely to stir up sediment from the bed and deposit it again elsewhere when the velocity decreases again. This is contrary to the effects of other residual currents, which can vary over time but are usually pointed in one direction. Campmans (2018) investigated the effects of (wind-) waves on sand wave dynamics, and found that they can enhance sand wave migration caused by other processes. As waves were not included, the question that remains is how large the influence of these waves would be relative to the wind and atmospheric pressure induced residual currents considered in this thesis.

In order to quantitatively assess this influence, a simple calculation of the bed shear stress due to waves is performed and compared to the bed shear stresses induced by (residual) currents. Bed shear stress can be used as an indicator for sediment mobility. When a certain shear stress threshold is exceeded, sediment grains are set into motion. Sediment transport increases non-linearly with bed shear stress ($S \sim \tau^{1.5}$), the larger the bed shear stress the more sediment transport can be expected. The bed shear stress due to waves is computed for two different types of hydrodynamic conditions, one in which the waves are relatively high (during a storm) and one in which they are representative for calmer conditions. Values for wave characteristics were retrieved from the validation report on the Princess Elisabeth Zone Measurement Campaign (Caires et al., 2024). The measurement location used in this validation report is positioned roughly 16 km towards the northeast with respect to the Area Of Interest, and the bed levels are in the same order of magnitude. The measurement data in this report span from November 2022 to November 2023.

A.1. Bed shear stress formulation

Bed shear stress can be related to bed friction and flow velocity. As waves and currents exert different influences on these parameters, a different approach is required to determine the bed shear stresses due to waves compared to currents. Jonsson (1967) developed methods to calculate both. More deterministic formulations, such as the formulation of Van Rijn (2007) which is used in the NEMO model, are able to capture the interactions between waves and currents on the bed shear stress. These formulations are however too detailed and go beyond the scope of this section, which is to make a simple calculation for comparison.

The bed shear stress due to currents can be calculated as follows.

$$\tau_c = \rho c_f U^2$$

In which,

ρ	average water density	$\mathrm{kg/m^3}$
c_f	friction factor due to currents	-
U	depth-averaged velocity	$\mathrm{m/s}$

The friction factor is computed as follows,

$$c_f = \frac{g}{C^2}$$

In which,

g	gravitational acceleration	$\mathrm{m/s^2}$
C	Chézy coefficient	-

The Chézy coefficient follows from,

$$C = 18 \log \frac{12d}{r}$$

In which,

d	water depth	m w.r.t. MSL
r	roughness height	m

The bed shear stress due to currents is calculated using a depth-averaged flow velocity into a certain direction. Under waves, the bed shear stress changes over time and is subject to the direction of the orbital velocity at that time. Hence, the magnitude of the maximum bed shear stress due to waves can be described as follows,

$$\hat{\tau}_w = \frac{1}{2} \rho f_w \hat{u}_0^2$$

In which,

f_w	friction factor under waves	-
$\hat{u}_0$	maximum orbital velocity at top of wave boundary layer	$\mathrm{m/s}$

The waves-only friction factor f_w can be calculated using the expression of Jonsson (1967), rewritten by Swart (1974),

$$f_w = \exp\left[-5.977 + 5.213 \left(\frac{\hat{\xi}_0}{r}\right)^{-0.194}\right]$$

$$f_w = 0.30 \quad \text{for} \quad \left(\frac{\hat{\xi}_0}{r}\right) < 1.59$$

$$\hat{\xi}_0 = \frac{\hat{u}_0 T}{2\pi}$$

In which,

T	wave period	s

From linear wave theory the amplitude of the near-bed wave-induced orbital velocity can be calculated,

$$\hat{u}_0 = \frac{\pi H}{T} \frac{1}{\sinh kd}$$

In which,

H	wave height	m
k	wave number	m^{-1}

A.2. Bottom shear stress during storm conditions

In order to relate the bed shear stress caused by waves to the bed shear stress caused by currents, a storm condition is considered. The bed shear stresses due currents during a storm are calculated using input of the NEMO model. The storm modelled in the NEMO model occurred on the 9th of February 2020. An overview of the input for the calculation of the bed shear stress due currents is shown below.

ρ	average water density	$1023\ \mathrm{kg/m^3}$
U_{tide}	maximum depth-averaged tidal velocity during storm Ciara in the AOI	$0.98\ \mathrm{m/s}$
U_{total}	maximum depth-averaged total velocity due to storm Ciara in the AOI	$1.39\ \mathrm{m/s}$
g	gravitational acceleration	$9.81\ \mathrm{m/s^2}$
d	water depth in trench	$34\ \mathrm{m\ w.r.t.\ MSL}$
r	roughness height (used in NEMO model)	$0.01\ \mathrm{m}$

Using these parameters as input provides the following bed shear stresses due to tide and the residual currents.

$$\tau_{c\_tide} = 1.40\ \mathrm{N/m^2}$$
$$\tau_{c\_total} = 2.82\ \mathrm{N/m^2}$$

These values also roughly coincide with the observed maximum bed shear stresses in the AOI during storm Ciara in the NEMO model ($\tau_{c\_tide} = 1.74\ \mathrm{N/m^2}$, and $\tau_{c\_total} = 3.56\ \mathrm{N/m^2}$).

The data for the wave characteristics are retrieved from the validation report on the Princess Elisabeth Zone Measurement Campaign. The highest waves were observed on the 10th of March in 2023 during storm Larisa. During the storm the waves originated from the southwest, and were hence headed in the same direction as the residual currents during storm Ciara. The other parameters are kept the same as in the calculation of the bed shear stress due to currents. The wave number k is calculated using the wave period and the dispersion relation.

H_s	highest significant wave height in observation data	$5.2\ \mathrm{m}$
T	wave period during highest significant wave height	$9.7\ \mathrm{s}$

Using these values as input provides the following maximum bed shear stress due to waves.

$$\hat{\tau}_w = 5.47\ \mathrm{N/m^2}$$

A.3. Bottom shear stress during representative hydrodynamic conditions

In this part the bed shear stresses due to waves during representative hydrodynamic conditions will be evaluated. The validation report on the Princess Elisabeth Zone Measurement Campaign was used to

retrieve the wave characteristics during representative hydrodynamic conditions. These are mentioned below.

H_s	most observed significant wave height in observation data	$1.2\ \mathrm{m}$
T	most observed wave period in observations data	$6\ \mathrm{s}$

Using these values as input provides the following maximum bed shear stress due to waves.

$$\hat{\tau}_w = 0.08\ \mathrm{N/m^2}$$

A.4. Reflection

The calculations performed in this appendix are done to quantitatively relate the influence of waves on the morphological interaction between sand waves and trenches to the influence of residual currents. It is found that during storm conditions the bed shear stresses caused by waves are a factor 2 higher than those caused by the tidal current and residual currents. During representative calm wave conditions, the influence on bed shear stress is very limited. In interpreting these findings, the following should be kept in mind.

Waves stir up sediment from the bed, and currents transport sediment over longer distances. These are two different types of transport mechanisms, hence two different bed shear stress formulations are used. This should be taken into account when comparing the two types of bed shear stresses. On top of this, two different storms are evaluated because the measurement data of the waves were not available in the period of the NEMO model. Storm Ciara resulted in the highest residual currents in a three year period, whereas the significant wave heights considered were amongst the highest observed in a one year period. The waves and residual currents are pointed in the same direction, which indicates that the storms are comparable. It is unknown how the storms exactly relate to each other, but both were severe storms. Last but not least, the bed shear stresses were now evaluated without accounting for the interaction between the currents and waves. This means that the calculated bed shear stresses due to waves are generated solely due to waves, without influence of the tide. As bed shear stresses increase non-linearly with flow velocity, it is expected that if the waves exerted their influence during maximum tidal and residual currents that an even larger increase in bed shear stress could occur.

Keeping these implications in mind, a judgement can be made on the expected influence of waves on the morphological interaction between sand waves and trenches. During a storm, the bed shear stresses due to waves are almost doubled compared to the bed shear stresses due to the total currents. This is higher, but not disproportionate. According to Campmans (2018) this increase in bed shear stress will likely result in larger sediment transport rates, and hence more sediment infilling into the trench. The 66% increase in sediment infilling during the peak tidal cycle of the storm would therefore likely be higher. However, when relating this increase in sediment infilling to the influence the tide has on a daily basis it is still expected that these magnitudes will be negligible over longer periods of time. During representative conditions the bed shear stress caused by the waves are several orders of magnitudes smaller than the bed shear stress caused by the tide, hence these are not expected to influence the system significantly.